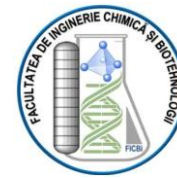




**THE NATIONAL UNIVERSITY OF
SCIENCE AND TECHNOLOGY
POLITEHNICA BUCHAREST**



Doctoral School of Chemical Engineering and Biotechnologies
Decision nr. ____ from ____

PhD THESIS

SUMMARY

Modification of titanium implantable surfaces with bioinspired structures

Author: Ing. Angela Gabriela OLARU (căs. PĂUN)

PhD supervisor: Prof.Dr. Ing. Cristian Pîrvu

PhD COMMITTEE

President	Prof. Dr. Ing. Ileana RĂU	from	The National University Of Science And Technology Politehnica Bucharest
PhD supervisor	Prof. Dr. Ing.Cristian PÎRVU	from	The National University Of Science And Technology Politehnica Bucharest
Referent	Prof. Dr. Cristina PÎRVU	from	University of Medicine and Pharmacy "Carol Davila" Bucharest
Referent	Conf. Dr. Elena VULPAȘU	from	Technical Construction University of Bucharest
Referent	Conf. Dr. Simona POPESCU	from	The National University Of Science And Technology Politehnica Bucharest

PART I. CURRENT STATE OF KNOWLEDGE IN THE FIELD	<u>1</u>
INTRODUCTION	<u>1</u>
CHAPTER I.	<u>8</u>
METALLIC BIOMATERIALS USED IN ORAL IMPLANTOLOGY	<u>8</u>
I.1. General information	<u>8</u>
I.2. Titanium use in dental applications	<u>12</u>
I.3. Risk of infection in oral implantology	<u>13</u>
I.3.1. <i>Generalities</i>	<u>13</u>
I.3.2. <i>Antibacterial compounds to prevent infection</i>	<u>15</u>
CHAPTER II.	<u>18</u>
SURFACE MODIFICATION METHODS OF METALLIC MATERIALS	<u>18</u>
II.1. Types of surface modification	<u>18</u>
II.2. Surface modification methods of metallic titanium and titanium alloy biomaterials by nanostructuring	<u>20</u>
II.2.1. Electrospinning method	<u>20</u>
II.2.2. Anodic oxidation method	<u>21</u>
II.3. Natural biopolymers used for titanium surfaces modification	<u>26</u>
II.3.1. Silk fibroin	<u>26</u>
II.3.2. Dopamine	<u>27</u>
CHAPTER III.	<u>30</u>
CHARACTERIZING BIOMATERIALS METHODS	<u>30</u>
III.1. Structural and composition analyzes	<u>30</u>
III.2. Electrochemical investigation methods	<u>36</u>
GENERAL OBJECTIVE OF THE THESIS	<u>41</u>
PART II. ORIGINAL CONTRIBUTIONS	<u>45</u>
CHAPTER IV.	<u>45</u>
MATERIALS AND METHODS USED	<u>45</u>
IV.1. Materials	<u>45</u>
IV.2. Modification methods	<u>46</u>
IV.2.1. Electrochemical deposition of TiO ₂ nanostructures on titanium surface	<u>46</u>
IV.2.2. Silk fibroin extraction (SF)	<u>50</u>
IV.2.3. SF deposition on the titanium surface	<u>51</u>
IV.2.4 Dopamine deposition on titanium surface by self-polymerization	<u>53</u>

IV.2.5. SF solution functionalization with zinc oxide nanoparticles (SF-nZnO)	<u>54</u>
IV.2.6. nZnO deposition on the titanium surface	<u>54</u>
IV.2.7. Amoxicilline deposition on the titanium surface	<u>55</u>
IV.3. CHARACTERIZATION METHODS	<u>55</u>
CHAPTER V.	<u>57</u>
IMPLANTABLE MATERIALS SURFACE MODIFICATION WITH SILK FIBROIN AND POLYDOPAMINE FOR AMOXICILLIN ENCAPSULATION	<u>57</u>
V.1. Introduction	<u>57</u>
V.2. Methods	<u>57</u>
V.3. Surface characterization	<u>57</u>
V.3.1. Surface morphology analysis of Ti modified with PD, SF and Amx	<u>57</u>
V.3.2. Topography and wettability analysis of Ti surface modified with PD, SF and Amx	<u>58</u>
V.3.3. Vickers microhardness for Ti surface modified with PD, SF and Amx	<u>60</u>
V.3.4. FT-IR analysis for Ti surface modified with PD, SF and Amx	<u>61</u>
V.3.5. Electrochemical characterization of Ti surface modified with PD, SF and Amx	<u>65</u>
V.3.6. Release studies for Ti surface modified with PD, SF and Amx	<u>71</u>
V.3.7. In vitro antibacterial activity of modified surfaces	<u>74</u>
V.4. Conclusion	<u>77</u>
CHAPTER VI.	<u>79</u>
TITANIUM IMPLANTABLE SURFACES MODIFICATION WITH TiO₂ NANOSTRUCTURES FOR THE AMOXICILLIN RELEASE	<u>79</u>
VI.1. Introduction	<u>79</u>
VI.2. Methods	<u>79</u>
VI.3. Surface characterization	<u>79</u>
VI.3.1. Surface morphology analysis of Ti modified with TNT, TNTr and Amx	<u>79</u>
VI.3.2. FT-IR analysis for Ti surface modified with TNT, TNTr and Amx	<u>81</u>
VI.3.3. Wettability analysis of Ti surface modified with TNT, TNTr and Amx	<u>81</u>
VI.3.4. Electrochemical characterization of Ti surface modified with TNT, TNTr and Amx	<u>82</u>
VI.3.5. Release studies for Ti surface modified with TNT, TNTr and Amx	<u>86</u>
VI.3.6. In vitro antibacterial activity of modified surfaces	<u>89</u>
VI.4. Conclusion	<u>90</u>
CHAPTER VII.	<u>93</u>
TI IMPLANTS SURFACES MODIFICATION WITH TiO₂ NANOTUBES/ SILK FIBROIN /NZNO FOR ENHANCED ANTIMICROBIAL EFFECT	<u>93</u>

VII.1. Introduction	<u>93</u>
VII.2. Methods	<u>93</u>
VII.3. Surface characterization	<u>94</u>
VII.3.1. Morphology and compositional analysis for Ti surface modified with TNT, SF, PD și nZnO	<u>94</u>
VII.3.2. Wettability and topography analysis of Ti surface modified with TNT, SF, PD and nZn	<u>96</u>
VII.3.3. FT-IR analysis for Ti surface modified with TNT, SF, PD and nZnO	<u>98</u>
VII.3.4. Electrochemical characterization of Ti surface modified with TNT, SF, PD and nZnO	<u>99</u>
VII.3.5. In vitro antibacterial activity of modified surfaces	<u>106</u>
VII.4. Conclusion	<u>110</u>
CHAPTER VIII.	<u>113</u>
TITANIUM SURFACE HYBRID COATING WITH REDUCED TiO₂ NANOTUBES/ SILK FIBROIN/ NZNO FOR IMPROVED ANTIBACTERIAL EFFECT	<u>113</u>
VIII.1. Introduction	<u>113</u>
VIII.2. Methods	<u>113</u>
VIII.3. Surface characterization	<u>113</u>
VIII.3.1. SF and SF-nZnO electrodeposition	<u>113</u>
VIII.3.2. Morphology and composition analysis of Ti surfaces modified with TNT, TNTr, SF and nZn	<u>114</u>
VIII.3.3. FT-IR analysis for Ti surface modified with TNT, TNTr, SF și nZnO	<u>117</u>
VIII.3.4. Wettability and topography analysis of Ti surface modified with TNT, TNTr, SF and nZn	<u>118</u>
VIII.3.5. Electrochemical characterization of Ti surface modified with TNT, TNTr, SF and nZnO	<u>120</u>
VIII.3.6. In vitro antibacterial activity of modified surfaces	<u>124</u>
VIII.4. Conclusion	<u>129</u>
CHAPTER IX.	<u>131</u>
CONCLUSIONS AND PERSPECTIVES	<u>131</u>
IX.1. General conclusions	<u>131</u>
IX.2. Perspectives	<u>133</u>
BIBLIOGRAPHY	<u>134</u>

INTRODUCTION

One of the most serious problems in human health care worldwide is the repair of bone defects [1-3]. They are caused by aging, accidents, sports injuries, fractures, bone tumors, external trauma, bone deformation, neoplastic diseases, osteoporosis and bone infection [2-12]. Despite the remarkable self-healing capacity of bone, healing bone defects remains a challenge, especially in the absence of medical intervention. From a clinical point of view, the golden treatment to resolve such large-scale bone defects is to fill the defect with an autologous or allogeneic bone graft to restore its structure and function [6]. Currently, autologous bone grafting has many problems, such as the limited number of bone grafts, secondary trauma to patients, and donor site morbidity. In addition, allogeneic bone possesses a number of limitations, such as reduced biological activity, immune rejection, and transmission of pathogens, which affect bone formation and cause bone resorption [4, 6, 9, 13]. Therefore, tissue engineering was developed, which is defined as "an interdisciplinary field that applies the principles of engineering and life sciences to the development of biological substitutes that restore, maintain, or improve tissue function" [14, 15]. Its purpose is to combine engineered materials, their interaction with cells, and appropriate biochemical and physicochemical factors to promote bone repair, replacement, or regeneration [5, 14, 16-19]. Biomaterials are critical factors for bone tissue engineering strategies and form the framework for tissue regeneration [18]. The availability of suitable biomaterials for the framework support is the key condition for the successful construction of any biological graft or modified tissues/organs. Biocompatibility, tissue mechanical strength, release or inter-communication of indispensable elements or signals, and adverse immune response are the major challenges in the successful implementation of implant-reproduced graft for medical purposes [17].

The field of biomaterials presents an extraordinary evolution in obtaining microstructures and nanostructures, with unlimited perspectives in research and biomedical applications. Biomaterials are used more and more often due to direct contact with living matter, a fact that determines the need to know the behavior of organisms towards them. The organism's response is either rejection or partial acceptance. In order to improve the health status of human organisms, numerous composite materials and various surface modifications are used that determine obtaining superior properties [20].

Metallic materials have been widely used in biomedical applications with internal body support and biological tissue replacement [21, 22]. The development of metal implants was primarily driven by the countless requests for bone restoration, usually the fixation of internal fracture of long bones [20]. Today, such medical implants can find applications in orthopedics, cardiovascular stents, pacemakers, defibrillators, neural prostheses, dentistry or drug delivery systems that can allow the normal functioning of several parts of the human body [23, 24]. However, like any other surgery, implanting a medical device into a patient's body comes with its own set of risks and complications. Bacterial colonization can occur on every implanted medical device, affected by a complex interaction between microorganisms, the implant surface, and host defense mechanisms. In the presence of an implanted medical device, such as an orthopedic prosthesis, an electronic cardiac device, an artificial heart valve or an indwelling catheter, the risk of infection is significantly increased [25, 26]. These infections pose a major risk to the health of patients and the proper functioning of medical devices. The attachment, colonization and proliferation of bacteria on the surface of medical devices is considered a root cause. Simple adherence of planktonic bacteria to the surface of the implanted device results in the formation of biofilms and bacterial cells that produce an extracellular polysaccharide matrix. This matrix protects them from the immune system of the host organism and becomes extremely resistant to antibiotics and anti-inflammatories [27].

Thus, to obtain a biomaterial, an interdisciplinary approach is needed. The types of biomaterials used, the types of modifications that can be made to them, but also the type of biomedical application must be considered. Creating biomedical devices with surfaces modified with antibiotics or antibacterial materials can prevent the occurrence of infections or inflammations on the surface of the devices. These surface-modified devices are capable of delivering biomedical substances, whose main function is to prevent, treat and reduce inflammation and infection [27].

Keywords: *Silk fibroin, Polydopamine, Reduced and unreduced TiO₂ nanotubes, Amoxicillin, ZnO nanoparticles.*

The main objective of the thesis is: elaboration of titanium-based metallic biomaterials with modified surfaces. Aiming to obtain the best performing biomaterials, their surface was modified with TiO₂ nanostructures and natural polymers. Taking the advances of their presence, it is possible to incorporate materials with an antibacterial effect (amoxicillin, ZnO nanoparticles). They are used in the medical industry, in particular, to prevent bacterial infections.

The objectives of this thesis are:

- Modification of implantable titanium surfaces with structures with antibacterial effect;
- Modification of the titanium surface with antibacterial compounds (amoxicillin), using biomimetic polymers inspired by nature (dopamine and silk fibroin);
- Testing the ability of silk fibroin and polydopamine layers to load and release amoxicillin, as well as testing the antibacterial effect;
- Obtaining unreduced and reduced TiO₂ nanotubes on titanium substrate, in organic electrolytes containing a viscous organic compound (EG), distilled/oxygenated water and ammonium fluoride (NH₄F);
- Optimization of reduced TiO₂ nanotubes to achieve a uniform (honeycomb-like) morphology and increased conductivity;
- Modification of unreduced and reduced TiO₂ nanotubes with amoxicillin for increased antibacterial activity;
- Deposition of silk fibroin fibers on TiO₂ nanotubular surfaces using the electrospinning process;
- Binding of zinc oxide nanoparticles through different coating methods, using silk fibroin fibers;
- Electrodeposition of silk fibroin functionalized with zinc oxide nanoparticles on unreduced and reduced TiO₂ nanotube modified titanium surfaces;
- Testing of titanium modified surfaces in terms of morphology, topography, wettability, electrochemical stability and antibacterial activity;

The work is structured in two parts: Part I. The current state of knowledge in the field and Part II. Original contributions.

Part I is assigned to the study from the specialized literature and includes 3 chapters in which the most recent data in the field addressed are highlighted.

- Chapter 1 presents data from the literature regarding the need to use dental implants, the properties and characteristics of titanium and its alloys, as well as the antibacterial compounds used to prevent infection.
- Chapter 2 presents the methods of modifying metallic biomaterials in order to obtain surfaces with improved characteristics.
- Chapter 3 presents the investigation methods used to characterize the obtained surfaces.

Part II is devoted to the original experimental results in 5 chapters, and in chapter 9 the general conclusions of the thesis are presented.

- In chapter 4, both the materials used for the experimental part and the methods used to obtain the modified titanium surfaces are described.
- Chapter 5 presents the results obtained following the modification of the titanium surface with polydopamine and silk fibroin in order to bind amoxicillin. These structures were characterized in terms of morphology, topography, electrochemical stability and antibacterial activity against three microorganisms (*Escherichia coli*, *Streptococcus mutans* and *Limosilactobacillus fermentum*).
- Chapter 6 includes the elaboration of unreduced and reduced TiO₂ nanotubes by the anodization method. These structures are functionalized with amoxicillin, an antibacterial compound. These surfaces were tested from the point of view of morphology, wettability, electrochemical stability and time release of the therapeutic agent.
- In Chapter 7, the titanium surface is coated with TiO₂ nanotubes, followed by the deposition of silk fibroin fibers using an electrospinning process. An important aspect of originality for this work lies in the approach and optimization of different methods of coating the functionalization process with ZnO, as an antibacterial agent. This was done using three hybrid coating methods and the resulting properties were comparatively evaluated in terms of morphology, topography, wettability, chemical stability and antibacterial effect against two microorganisms (*Staphylococcus aureus* and *Enterococcus faecalis*).
- In Chapter 8, the surface of unreduced and reduced TiO₂ nanotubes is modified by the electrochemical deposition of silk fibroin functionalized with ZnO nanoparticles, thus contributing to obtaining new surfaces with increased

antibacterial effect. These surfaces were characterized morphologically, topographically, electrochemically and the antibacterial effect against two microorganisms (*E. coli* și *S. aureus*).

This doctoral thesis concludes with Chapter 9, "Conclusions and perspectives", which summarizes the main original results discussed throughout the chapters of the second part of the thesis, and the perspectives for further research.

The Appendix presents the dissemination of the original results at international conferences and mentions the articles published in the Scientific Bulletin of the U.P.B. and those accepted at ISI journals.

CHAPTER IV. MATERIALS AND METHODS

IV.1. MATERIALS

In this subsection, all the materials used for the experimental part were presented.

IV.2. METHODS

IV.2.1. Electrochemical deposition of TiO₂ nanostructures on titanium surface

IV.2.1.1. Obtaining TiO₂ nanotubes (TNT)

NT deposited

The anodizing process was performed in the electrochemical cell with two-electrodes: a Ti as anode and a Pt electrode as cathode. Using a MATRIX MPS-7163 source, the voltage was increased from 0 to 40V or 80 V, with a speed of 2V / 10 seconds and then kept constant at room temperature. The samples were named **TNT-40V** și **TNT-80V**. The composition of the solution was chosen based on previous studies in our group [1, 2]. After anodizing the samples obtained were rinsed with distilled water and then calcined for 2 hours at 450°C.

IV.2.1.2. Obtaining reduced TiO₂ nanotubes (TNTr)

a. TNTr deposited

Subsequently, the anodized and calcined samples were subjected to an electrochemical reduction process. The samples were named **TNTr2** și **TNTr4**.

TNTr optimization

A. Sample structure and morphology

Comparing the morphology, surface conductivity and band gap energy, TNT-40V, TNT-80V and corresponding reduced TNTr2, TNTr4 samples were selected to be further functionalized with antibacterial agent.

IV.2.2. Extracția fibroinei de mătase (SF)

The fibroin extraction procedure was performed according to a protocol presented in the literature [3, 4]. Briefly, *B. mori* cocoons were chopped and boiled in 0.02 M sodium carbonate for 30 min and rinsed with distilled water 3 times for 20 minutes. After drying, the degummed SF was dissolved in 9.3M LiBr at 60 °C for 4 h. Then, the solution was dialyzed in distilled water using a cellulose dialysis membrane for 72h. The resulting silk fibroin solutions were stored at 4°C, having a concentration between 6% and 7.5%.

IV.2.3. Deposition of silk fibroin on the titanium surface

IV.2.3.1. SF deposition on Ti, TNT or TNTr surfaces by the electrochemical method

For electrodeposition process a 3% aqueous silk fibroin solution was used. The fibroin was deposited using chrono-amperometric method, in an electrochemical cell with 2 electrodes, on three substrates (Ti, TNT-40V și TNTr2). A voltage of 10 V for 10 minutes was applied. After electrodeposition, samples were immersed in a 90% methanol

solution for 15 minutes, to turn the fresh deposited fibroin into a water insoluble silk fibroin layer. Then, the samples were rinsed with water. Subsequently, the samples were stored in the freezer overnight, generating a gel coating with open porosity. They were named **Ti/SFech**, **TNT/SFech** și **TNTr/SFech**.

IV.2.3.2. SF deposition on TNT surfaces by the electrospinning method

a. SF deposition

Initially, a SF/PEO solution was obtained by combining a 4:1 volume ratio of 6.45% (w/v) silk fibroin aqueous solution with 5.0 % (w/v) polyethylene oxide (PEO). It resulted in a 3 % silk fibroin/PEO solution.

SF optimization

The silk fibers were deposited by the electrospinning method using as experimental parameters: **15kV, 15 cm, 0.75mL/h, 10 min**. Thus, using these parameters, fibers were deposited on the nanostructured surfaces. These were named **TNT/SFef**.

IV.2.4 Dopamine deposition on titanium surface by self-polymerization

TRIS buffer solution at pH 8.5 was prepared from distilled water, 0.2 M Trizma® and 0.2 M HCl.

IV.2.4.1. Dopamine deposition on titanium surface

In a sterile container, polished Ti samples were immersed for 24 h at room temperature in 10 mL polydopamine solution (9.45 g dopamine/L TRIS buffer pH 8.5). Samples were rinsed with distilled water. The resulted modified Ti substrate was named **Ti/PD**.

IV.2.4.2. Dopamine deposition on the surface of TNT

In a sterile container, TNT/SFef samples were immersed in 10 mL polydopamine solution (2 g dopamine/L TRIS buffer pH 8.5), for 8 h in dark at room temperature under constant shaking. The samples were washed using distilled water. These were named **TNT/SFef/PD**.

IV.2.5. Functionalization of SF solution with zinc oxide nanoparticles (SF-nZnO)

Firstly, a solution containing ZnO nanoparticles (0.02 wt.%), Triton X (0.01 % vol.) and distilled water was prepared.

This solution was added for a final concentration of 0.125% vol into aqueous solution of SF or SF/PEO with a concentration of 3%, being named **SFech-nZnO** sau **SFef-nZnO**.

IV.2.6. Deposition of nZnO on the titanium surface

IV.2.6.1. nZnO deposition by spin coating

100 μ L were extracted from the ZnO solution that had already been made. The spin coating method is used to deposit this solution on the TNT-40V or TNT/SFef/PD surfaces. The TNT-40V or TNT/SFef/PD substrates are fixed on a spin coater, and the disk speed is set to 3000 rpm for 30 seconds. Following that, the samples were calcined for 10 minutes at 180 °C. The samples were named **TNT/nZnO** sau **TNT/SFef/PD/nZnO**.

Silk fibroin fibers were deposited on TNT/nZnO samples under the same conditions (described in point IV.2.2.3) by the electrospinning method. The samples were named **TNT/nZnO/SFef**.

IV.2.6.2. Deposition of SF-nZnO by the electrochemical method

The previously obtained solution of SF-ZnO was electrochemically deposited on TNT_40V or TNTr2 substrates by applying 10 V for 10 minutes with an Autolab 302 N potentiostat-galvanostat (procedure described in

point VII.4.1.). For SF-ZnO film fixation, the samples were immersed in 90% methanol for 15 minutes. Subsequently, the samples were stored in the freezer for 24 hours. They were named **TNT/SFech-nZnO** or **TNTr/SFech-ZnO**.

IV.2.6.3. Deposition of SF-nZnO by the electrospinning method

The nZnO solution was added for a final concentration of 0.125 % vol. for ZnO into Silk fibroin/PEO solution. The fibers were deposited from this mixture by electrospun, under the conditions de-scribed in point VII.3.2. The resulting samples were named **TNT/SFef-nZnO**.

IV.2.7. Amoxicillin binding on the titanium surface

IV.2.7.1. Amoxicillin binding to Ti surface via polydopamine or fibroin

Ti, Ti/PD and Ti/SFech samples were immersed in 3g/L aqueous amoxicillin solution (pH 5.5) in sterile containers for 24 hours, at room temperature. Then, the samples were washed with distilled water to remove the excess of none adsorbed antibiotic. Amoxicillin loaded samples were named **Ti/Amx**, **Ti/PD/Amx** and **Ti/SFech/Amx**.

IV.2.7.2. Amoxicillin incorporation into TNT or TNTr nanostructures

Ti, TNT-40V, TNT-80V, TNTr2, TNTr4 samples were submerged in 10 mL of aqueous amoxicillin solution (3g/L) for 48 hours, at room temperature. The samples were then washed with distilled water to eliminate any unabsorbed antibiotic. Amoxicillin loaded samples were named **Ti/Amx**, **TNT-40V/Amx**, **TNT-80V/Amx**, **TNTr-40V/Amx** și **TNTr-80V/Amx**.

CHAPTER V. IMPLANTABLE SURFACE MODIFICATION WITH SILK FIBROIN AND POLYDOPAMINE FOR AMOXICILLIN ENCAPSULATION

This paper presents an approach to the interaction between Amx, PD, SF and the titanium surface, as well as testing the ability of silk fibroin and polydopamine coatings to load and release amoxicillin for the titanium dental implant surface. The two biopolymers were easily deposited on Ti surface by self-polymerization (PD) and electrodeposition (SF), two very simple techniques that do not involve expensive reagents or complex equipment.

V.3. SURFACE CHARACTERIZATION

V.3.1. Surfaces morphology analysis

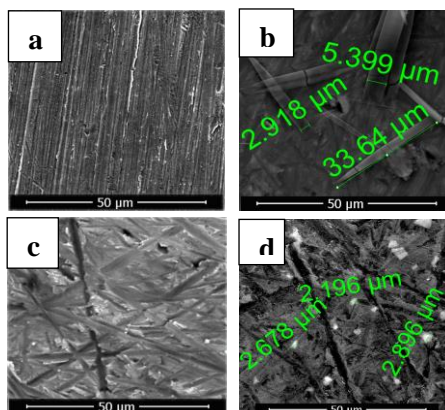


Fig. 5.1. SEM images corresponding to the coated Ti samples: a) Ti/PD; b) Ti/PD/Amx; c) Ti/SFech; d) Ti/SFech/Amx.

Fig. 5.1 shows the SEM images for Ti samples with modified surfaces. In Fig. 5.1a, the deposition of polydopamine can be observed as a thin and uniform film on the titanium surface, as the scratches remained after the polishing step are still visible. In Fig. 5.1b, Amx crystals, well anchored on the titanium surface through PD film, are

visible. These crystals have a tubular/acicular shape of different sizes, 2-5 μm in diameter and around few tens of micrometres in length.


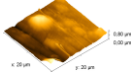
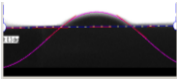
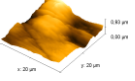

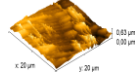
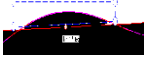
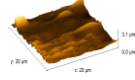
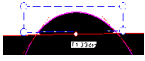
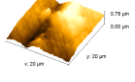
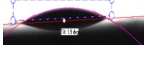
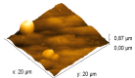
In Fig. 5.1c, a uniform electrodeposited SF layer on Ti substrate is visible. It seems thicker compared to PD film, transparent, and follows the conformity of the Ti surface. In Fig. 5.1d, Amx was deposited as agglomerates of 1 – 5 μm on the SF film, creating different shapes, comparing with those loaded on PD layer.

V.3.2. Topography and surface wettability analysis

The representative water droplet images are depicted in Table 5.1. . The contact angle for Ti-PD sample (55°) is lower compared to Ti substrate (75°), in good agreement with the result obtained in other studies [5, 6]. The contact angle for Ti-SF sample is close to the one recorded for Ti-PD sample, being also hydrophilic as was already observed in our previous study [7]. After Amx was grafted in the two films (PD and SF) the surface chemistry was changed and the value of the contact angle has consistently decreased to values between 10° to 20° . Similar results were also observed in the case of other antibiotic (cefotaxime sodium) deposited through polydopamine on Ti surface[5]. There is not a significant wettability difference between Ti/SFech/Amx and Ti/PD/Amx, both having a strong hydrophilic character, which could be beneficial for a better cells adhesion and proliferation on the implantable materials surface [8].

Ti/PD/Amx has an increased roughness compared to Ti/SFech/Amx surface. The difference between the morphologies of these two samples was also noticed from the SEM images, Fig. 5.1b și 5.1d. Amx AMX is visible as big crystals attached on polydopamine film and as small particles agglomerates on silk fibroin film. Comparing with Ti substrate, the roughness increases after surface modification for Ti-SF while the contact angle is decreasing. This is in agreement with Wenzel state [9]. For Ti/PD the contact angle is decreasing compared to substrate, but the roughness is also decreasing. This type of wetting behaviour called ‘mushroom state’ is an intermediate state between Cassie–Baxter model (trapped air is present between the textured surface and water droplet) and Wenzel model [9].

Table 5.1. The contact angle and roughness values.

Sample	Water droplet image	Angles values (degrees)	AFM 3D image	Rms [nm]
Ti		75 ± 0.15		116 ± 0.59
Ti/Amx		28 ± 0.38		231 ± 0.7
Ti/PD		55 ± 0.54		84 ± 0.32
Ti/PD/Amx		16 ± 0.91		239 ± 1.95
Ti/SFech		59 ± 0.91		165 ± 0.29
Ti/SFech/Amx		19 ± 0.99		110 ± 1.82

V.3.3. Vickers microhardness

For solid materials, hardness is a measure of the material’s resistance capacity to the permanent indentation or scratching. The degree of wear-damage is connected with the surface roughness, which is a method for quantifying the texture/topography of the worn surfaces [10]. It is observed that the values for uncoated and modified titanium are

almost similar, suggesting that the methods used for titanium surface modification does not have a significant influence on the titanium micro-hardness. The Ti/SF_{ech} sample has the highest standard deviation, suggesting a possible non-homogeneous surface.

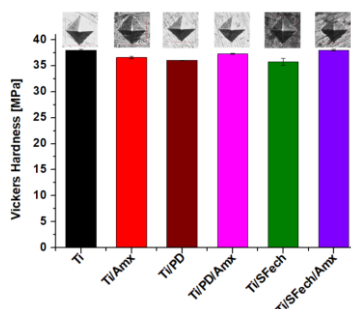


Fig. 5.2. Graphic representation of Vickers hardness.

V.3.4. FT-IR analysis

In our study, for the obtained silk fibroin solution 7.3%, the peaks at 1620, 1515 and 1227 cm^{-1} were assigned to amide I, II and III (Fig. 5.3a). For the Ti/SFech sample (Fig. 5.3b) it can be observed that it has approximately the same values for the peaks, as a proof that titanium surface was successfully coated with fibroin. The treatment with methanol after deposition, turns the fibroin random coils into β -sheets conformation, characteristic peaks being present at 1620 cm^{-1} , 1515 cm^{-1} , and 1233 cm^{-1} [11].

In Fig. 5.3c the infrared spectra of amoxicillin powder, peaks are found a 3458, 3166, 1768, 1685, 1580, 1480, 1392, 1315 and 1245 cm^{-1} [12]. It can be observed that the Ti/SFech/Amx and Amx powder (Fig. 5.3c și 5.3d) present similar peaks highlighting that amoxicillin was incorporated on the Ti/SFech surface.

In Fig. 5.3b and 5.3d, spectra corresponding to Ti/SFech and Ti/SFech/Amx were compared. In the Ti/SFech/Amx sample spectra, the specific silk fibroin peaks are attenuated, indicating that the amoxicillin was incorporated. The intense band at 1770 cm^{-1} attributed to the -C = O (carboxyl) stretching vibration in free amoxicillin [13] is also present in the case of Ti/SFech/Amx. Peaks corresponding to C-O-C and C-OH stretching vibration appeared at 1119 and 1076 cm^{-1} [14] and are also present in the case of Ti-SF/AMX sample, indicating a possible spontaneous conjugation of silk protein with amoxicillin.

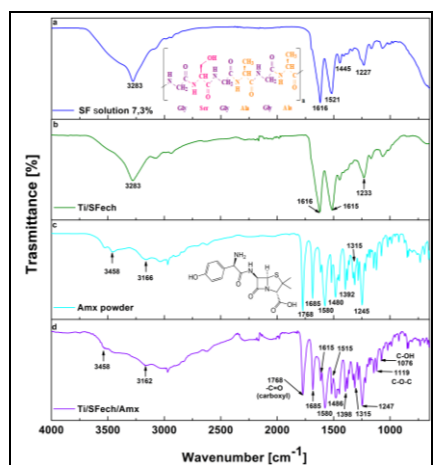


Fig. 5.3. FT-IR images corresponding to the samples: a) SF solution 7,3%; b) Ti/SF; c) Amx powder și d) Ti/SF/Amx.

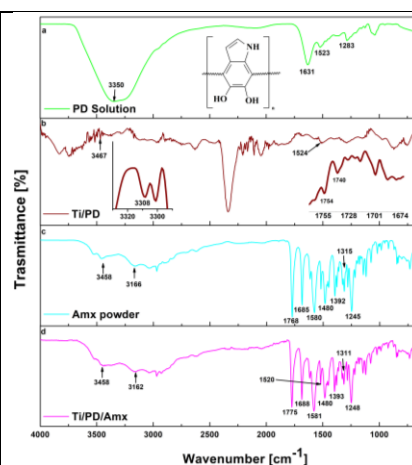


Fig. 5.4. FT-IR images corresponding to the samples: a) PD solution; b) Ti/PD; c) Amx powder și d)Ti/PD/Amx.

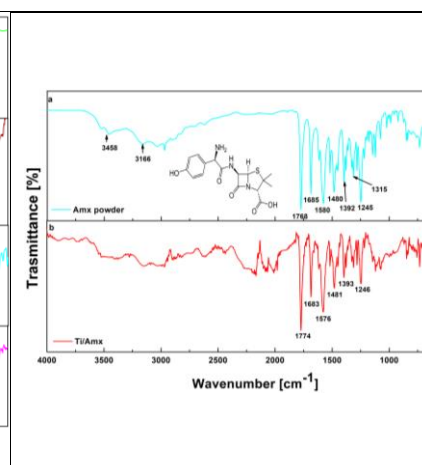


Fig. 5.5. . FT-IR images corresponding: a) Amx powder și b) Ti/Amx.

The infrared absorption spectra of polydopamine at 3350 cm^{-1} corresponds to the -OH and N-H stretches, Fig. 5.4a. Moreover, the peaks at 1283 cm^{-1} and 1631 cm^{-1} , are assigned to the stretching vibration of catechol hydroxyl C-O and C=O bonds. The peak at 1523 cm^{-1} is assigned to C=C bonds from the indole structure of PD [15, 16]. In the specific spectrum of the Ti/PD sample (Fig. 5.4b, the peaks are assigned as follows: peaks at 3308 and 3467 cm^{-1} for the -OH vibration Peaks at 1754 cm^{-1} and 1740 cm^{-1} are characteristic for the -NH vibration and stretching vibration of carbonyl group [6].

The peaks corresponding to the Amx powder, Fig. 5.4c, are also present in the spectra recorded for Ti/PD/Amx sample (Fig. 5.4d), demonstrating the presence of antibiotic i.

Spectra corresponding to Ti/PD (Fig 5.4b) and Ti/PD/Amx (Fig 5.4d) samples were compared. It is visible that peak at 1523 cm^{-1} assigned to the C=C bonds from the indole structure of PD is also present in the spectra of Ti/PD/Amx sample, shifted at 1520 cm^{-1} . The intense band at 1775 cm^{-1} is present in the case of Ti/PD/Amx sample, being attributed to the -C=O (carboxyl) stretching vibration of [13]. AMX possible interactions with polydopamine are $\pi\text{-}\pi$ interactions and hydrogen bonds, similar as it was described for other antibiotics [15, 17]. $\pi\text{-}\pi$ interactions can be with aromatic part of PD and hydrogen bonds between amino groups of amoxicillin and hydroxyl groups of PD.

Ti/Amx sample (Fig. 5.5b) presents similar peaks at 1774 cm^{-1} (-C=O carboxyl), 1683 cm^{-1} (-C=O amide), 1576 cm^{-1} (-NH), 1481 cm^{-1} (C=C aromatic), 1393 cm^{-1} (-OH bending) and 1246 cm^{-1} (-CO-) [44]. Amoxicillin powder spectra, Fig. 5.5a, presents peaks at the same wavenumbers so we can conclude that Amx is present on the Ti surface.

V.3.5. Electrochemical characterization

V.3.5.1. Tafel analysis

Fig. 5.6 shows the Tafel diagrams for the obtained samples. All coated samples have lower corrosion currents and more electropositive potentials than Ti substrate, so they are less susceptible to corrosion.

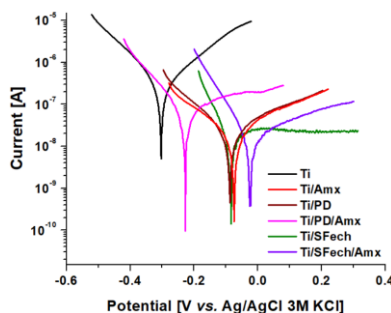


Fig. 5.6. Tafel diagram corresponding to the uncoated and coated Ti samples, recorded in Fusayama saliva.

The corresponding Tafel slopes for the Ti substrate and modified electrodes, obtained at room temperature, were calculated based on the polarization curves using Nova software. The obtained results were 159 mV/dec - Ti; 192 mV/dec - Ti/Amx; 141 mV/dec - Ti/PD; 302 mV/dec - Ti/PD/Amx; 136 mV/dec - Ti/SFech and 159 mV/dec - Ti/SFech/Amx. The slopes found for all electrodes are higher than 120 mV per decade, suggesting that the Volmer step could be the rate-determining step [18]. From corrosion current, protection efficiency was calculated using formula described in literature [19]. We obtained the following results 82% - Ti/Amx; $86,4\%$ - Ti/PD; $69,84\%$ - Ti/PD/Amx; $96,88\%$ - Ti/SFech and $94,32\%$ - Ti/SFech/Amx. The efficiency is higher than 60% for all samples.

Table 5.2. The main corrosion parameters.

Samples	Corrosion potential [V]	Corrosion current density [A/cm^2]	Corrosion rate [mm/year]
---------	-------------------------	--	--------------------------

Ti	-0.30	$12.50 \cdot 10^{-7}$	$109.07 \cdot 10^{-4}$
Ti/Amx	-0.07	$2.25 \cdot 10^{-7}$	$19.32 \cdot 10^{-4}$
Ti/PD	-0.09	$1.70 \cdot 10^{-7}$	$14.8 \cdot 10^{-4}$
Ti/PD/Amx	-0.23	$3.77 \cdot 10^{-7}$	$32.65 \cdot 10^{-4}$
Ti/SFech	-0.08	$0.39 \cdot 10^{-7}$	$3.42 \cdot 10^{-4}$
Ti/SFech/Amx	-0.02	$0.71 \cdot 10^{-7}$	$6.19 \cdot 10^{-4}$

From the corrosion point of view, the Ti/SFech sample is the most stable, having the lowest corrosion rate, being approximately 32 times lower compared to Ti uncoated substrate. Ti/PD has also low corrosion current density and a lower corrosion rate compared to Ti substrate. Other studies also reported increased corrosion protection in the case of fibroin coatings [20] or polydopamine coatings [21].

For Ti/Amx the corrosion rate is lower than in the case of the Ti sample, Amx behaving as a protective coating for the Ti surface. On contrary, by loading Amx on the Ti substrate covered with SF and PD films, the corrosion rate and corrosion current densities increased probably due to the interaction between Amx and the two polymers observed in the FTIR analysis, and also, probably due to the differences in the morphologies of the films. The lower corrosion rate was obtained for the samples with fibroin film, this film is covering the entire surface, creating a supplementary barrier that protect the substrate. However, the corrosion rate for Amx- modified samples are significantly lower comparing with uncoated titanium.

V.3.5.2. Impedance diagrams

In Fig. 5.7 are presented normalized Nyquist diagrams corresponding to the modified surface samples and the untreated titanium, recorded at OCP. All coated samples, including the ones with AMX, have higher resistance being more stable than Ti substrate.

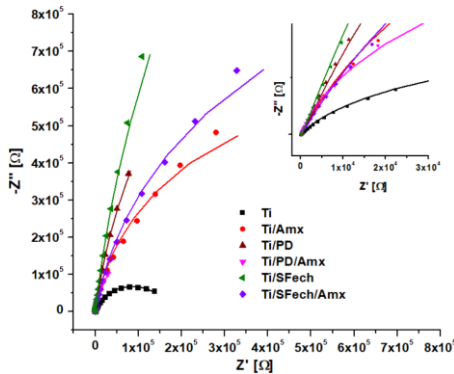


Fig. 5.7. Nyquist diagrams for uncoated and coated Ti samples, recorded in Fusayama saliva.

Table 5.3 comprises the data obtained using the Nova software. The solution resistance is almost similar for all tested samples, around 100Ω , considering the similarity of electrolyte and test conditions. It is noticed that after surfaces modification, the resistance of the native barrier oxide layer increases compared with that of Ti. The total resistance ($R_t = R_{\text{coating}} + R_{\text{oxide}}$) corresponding to Ti/SFech sample has a higher value of $8.054 \cdot 10^6 \Omega$, compared to Ti/PD sample, which is $3.618 \cdot 10^6 \Omega$. These values are in good correlation with the results from Tafel slope, where Ti/SFech sample presented a lower corrosion rate compared to Ti/PD sample.

By simply loading the AMX on the PD film (Ti/PD/Amx sample) and SF film (Ti/SFech/Amx sample), the resistance of the native oxide layer decreases compared with the one for Ti/PD and Ti/SFech sample, but it is higher than the uncoated Ti. Ti/Amx sample has a lower resistance of the coating compared to Ti/PD/Amx and Ti/SF/Amx samples. The changes in electrochemical behaviour that were observed for the samples loaded with amoxicillin could be associated with the nitrogen-containing β -lactam ring that acts as a reducing agent, as it was observed in other study [22].

In our case all N values for native oxide layer are around 0.9, thus indicating a pseudocapacitive behaviour. For coating layer, N has values between 0.3 and 0.45 indicating pseudo-resistive coatings.

Table 5.3. Parameters of proposed equivalent circuits

Parameters Samples	R_s [Ω]	R_{coating} [Ω]	CPE_{coating}		R_{oxide} [Ω]	CPE_{oxide}		X^2
			Y_0	N		Y_0	N	
			[S^*s^n]			[S^*s^n]		
Ti	84.41	-	-	-	$0.17 \cdot 10^6$	$2.91 \cdot 10^{-5}$	0.85	0.05
Ti/Amx	98.84	$0.02 \cdot 10^4$	$0.07 \cdot 10^{-4}$	0.42	$1.23 \cdot 10^6$	$1.83 \cdot 10^{-5}$	0.92	0.04
Ti/PD	106.35	$1.75 \cdot 10^4$	$7.88 \cdot 10^{-4}$	0.45	$3.61 \cdot 10^6$	$3.42 \cdot 10^{-5}$	0.94	0.01
Ti/PD/Amx	86.63	$0.37 \cdot 10^4$	$32.61 \cdot 10^{-4}$	0.40	$0.52 \cdot 10^6$	$4.73 \cdot 10^{-5}$	0.95	0.04
Ti/SFech	85.64	$0.37 \cdot 10^4$	$12.50 \cdot 10^{-4}$	0.32	$8.05 \cdot 10^6$	$1.90 \cdot 10^{-5}$	0.94	0.01
Ti/SFech/Amx	90.17	$0.14 \cdot 10^4$	$14.82 \cdot 10^{-4}$	0.33	$1.95 \cdot 10^6$	$1.41 \cdot 10^{-5}$	0.91	0.07

V.3.5.3. Cyclic voltammetry

The obtained C_{dl} values are presented in the Table 5.4.

After the mussel-inspired titanium surface modification with polydopamine, the value of C_{dl} increases from 215 to 500 $\mu\text{F}/\text{cm}^2$. The pseudo-capacitance induced by the greater number of redox-active groups of PD could explain this increase in the capacitance [23, 24].

The same C_{dl} increase was also observed for titanium surface modification with fibroin, but the difference is not as large as in the case of polydopamine. SF usually refolds to a more ordered state, β -sheet structure, which is tighter and more compact, reducing the amount of negative charge caused by the protonation of carboxyl groups [25-27].

Table 5.4. C_{dl} values calculated from CV plots for Ti and coated samples.

Sample	C_{dl} [$\mu\text{F}/\text{cm}^2$]
Ti	214.81
Ti/Amx	264.07
Ti/PD	500.86
Ti/PD/Amx	641.85
Ti/SFech	383.79
Ti/SFech/Amx	693.73

After the Amx loading on the Ti-SF surface, the value of C_{dl} increases with about 300 $\mu\text{F}/\text{cm}^2$ probably due to the spontaneous conjugation of silk protein with amoxicillin as was revealed by FT-IR analysis. The protons, in our case from the Fusayama solution (pH 6.5), weaken the tight structures of SF by gradually breaking the hydrogen bonds in sheet structures [27], probably causing the increasing the active surface and improving the double layer formation.

Although Ti/PD binds a larger amount of Amx compared to Ti/SFech, the C_{dl} increase for Ti/PD/AMX is smaller, being only with 142 $\mu\text{F}/\text{cm}^2$ higher than Ti-PD. Thus, even if AMX comes with an important contribution of charged functional groups, it seems that the hydrogen bonds between amino groups of AMX and hydroxyl groups of PD and π - π interactions between AMX and aromatic part of PD [15, 17] covers a part of the surface creating an impediment in formation of double layer.

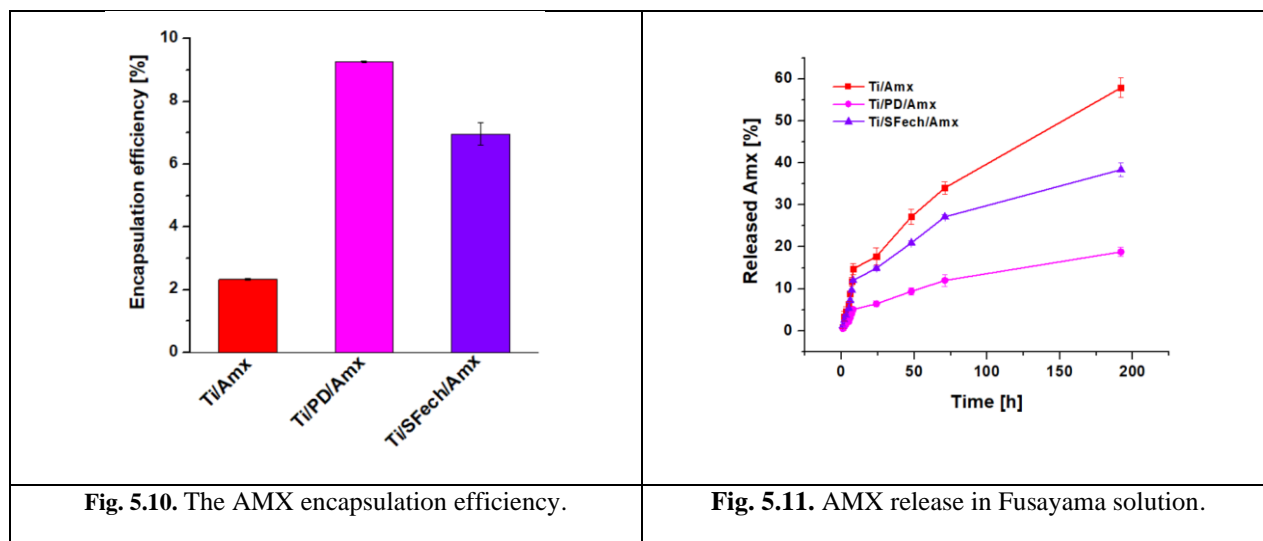
Electrochemical analysis highlighted the better stability of titanium modified sample and contributed to the establishing the interaction between amoxicillin, biopolymers and titanium surface.

V.3.6. In vitro amoxicillin release

Firstly, the encapsulation efficiency was evaluated considering the difference between the initial Amx concentration and the final Amx concentration, after the sample removing from the immersion solution.

In the case of uncoated Ti, an amount of 69.9 mg/cm^2 was adsorbed, representing 2.33% from the total Amx quantity. The highest quantity of Amx was loaded in the case of the Ti/PD sample, 277.8 mg/cm^2 , representing 9.26% from the total Amx quantity, probably due to a better interaction between Amx and PD by their functional groups and aromatic π - π interactions.

For Ti/SFech sample, the quantity of encapsulated Amx (by conjugation of silk protein with amoxicillin) was 208.8 mg Amx /cm², representing a percent of 6.96% (Fig. 5.10).



A sudden release, in the first hours of immersion in Fusayama saliva, was observed for all samples, Fig. 5.11. In the case of Ti/Amx and Ti/SFech/Amx samples, no significant differences were observed in the first 8 hours, the release of Amx being 14.73% and 12% respectively. The slowest release, 5.1% occurred in the case of the Ti/PD/Amx sample.

After 192 h, a drug release of 57,87%- Ti/Amx, 18,81%- Ti/PD/Amx and 38,37%- Ti/SFech/Amx.

The fibroin coating conducted in a slower release over time compared to the uncoated Ti, which had a faster release of the antibiotic. Amx was best incorporated on the surface of the Ti/PD/Amx sample, the use of the polydopamine as adhesive layer, ensuring a slower release over time. A possible explanation for Ti/SFech/Amx faster releasing compared to Ti/PD/Amx could be the pH and complex composition of Fusayama solution. These contributed to the hydrogen bond wakening from beta sheet configuration of SF structure as it was already presented in electrochemical tests.

In conclusion, the surface modification of Ti with the biopolymers influences the entrapment efficiency of amoxicillin and the release mechanism of this drug.

V.3.7. *In vitro* antibacterial assay

The results for the antibacterial assay against three selected microorganisms are shown in Fig. 11. It can be observed that after 24 h, all samples with Amx have quasi similar antibacterial effect. Consistent differences appeared after 96 h and 192 h. In the case of Ti/Amx sample, the antibacterial effect presents a sharp decrease over time. Compared to this, Ti/PD/Amx and Ti/SFech/Amx, have a higher antibacterial effect even after 192 h exposure, probably because the antibiotic was constantly released after the first day, ensuring a better antibacterial effect, comparing with Ti/Amx sample that encapsulated a small antibiotic quantity that is released rapidly.

The inhibition effect is more pronounced for the samples containing a polymer coating, and the maximum antibacterial activity was obtained for the samples in which polydopamine was used as coating for loaded Amx. The reason resides in a better adhesive function of the polydopamine, producing an efficient fixation of the antibiotic on the surface of titanium. Another possible reason is the synergistic antimicrobial effect between the polydopamine and antibiotic since the polymer PD already proved its antibacterial effect in previous studies [28, 29]. Qiqi Lei and co-workers mentioned that the antibacterial ability was greatly improved when dopamine was present. A possible explanation is that polydopamine aggressively captures bacteria onto the surface, making contact-sterilization easier [30].

Although the best results were obtained for Ti/PD/Amx sample, the silk fibroin coating also represents an alternative for fixing the antibiotic onto the Ti surface, considering its apport in terms of bioactivity. However, since silk fibroin coatings possess suitable properties to be used frequently as scaffolds, medical device coatings or wound dressings, it was necessary an improvement of its poor antibacterial activity [31].

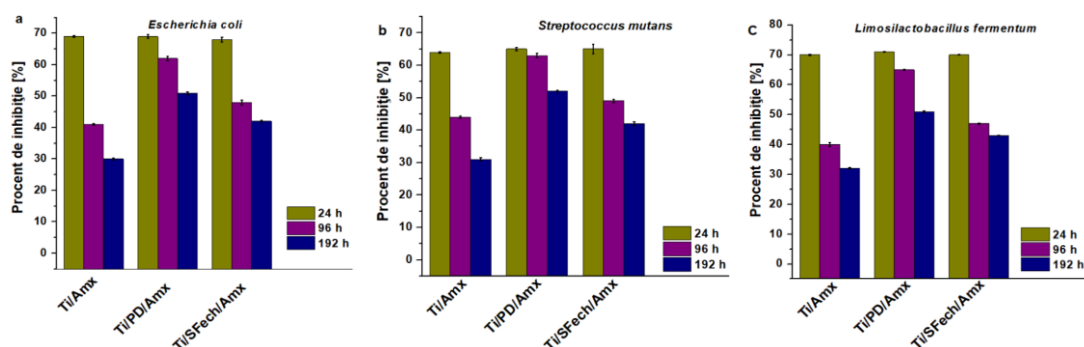


Fig. 5.12. Inhibitory efficiency, against: a) *Escherichia coli*; b) *Streptococcus mutans*; c) *Limosilactobacillus fermentum*.

CHAPTER VI. TITANIUM SURFACE MODIFICATION WITH TiO₂ NANOSTRUCTURES FOR AMOXICILLIN RELEASE IN DENTAL IMPLANTOLOGY

The present paper focuses to the amoxicillin binding on the Ti surface using unreduced or reduced TiO₂ nanotubes. This paper presents an approach to forming reduced TiO₂ nanotubes as well as testing their ability to incorporate and locally release amoxicillin for dental implantable titanium surfaces.

VI.3. SURFACE CHARACTERIZATION

VI.3.1. Surfaces morphology analysis

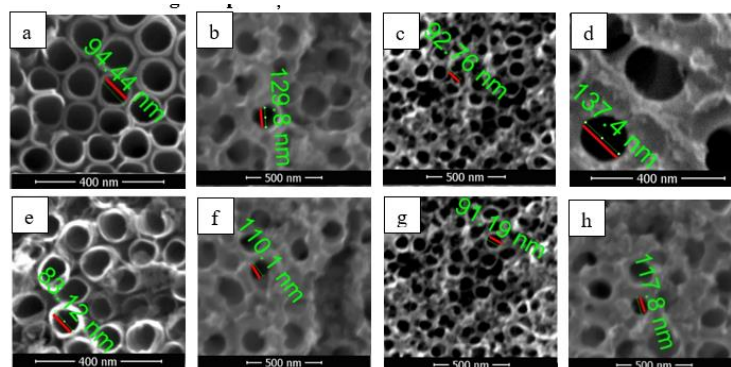


Fig. 6.1. SEM images corresponding to the nanostructured samples: a) TNT-40V; b) TNT-80V; c) TNTr2; d) TNTr4; e) TNT-40V/Amx; f) TNT-80V/Amx; g) TNTr-40V/Amx; h) TNTr-80V/Amx.

Fig. 6.1 shows SEM images of titanium dioxide nanotubes obtained by electrochemical anodization with and without amoxicillin. The surface of Ti samples is covered entirely with self-organized nanotubes that have different heights but uniform diameters. It can be seen that AMX does not influence the morphology of the nanotubes. The presence of amoxicillin on the nanotubes surface is not visible considering that a small amount of this compound was attached.

VI.3.2. Analiza FT-IR

As shown in Fig. 6.2, the N-H stretching, O-H stretching, C=O carboxyl, C=O amide, N-H bending, C=C, O-H bending, C-N bending and C-O groups can be identified in the infrared absorption spectra of amoxicillin powder at 3449, 3162, 1780, 1687, 1574, 1487, 1398, 1315, and 1252 cm⁻¹ [12]. Nanostructured samples modified with amoxicillin

(TNT-40V/Amx, TNT-80V/Amx, TNTr-40V/Amx și TNTr-80V/Amx) show the same peaks. This indicate that AMX was loaded on the nanostructured surfaces.

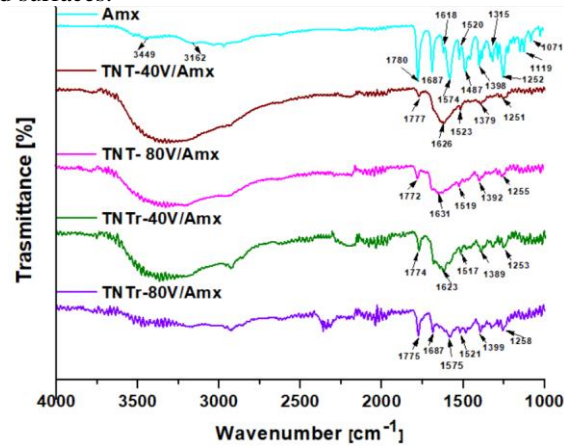
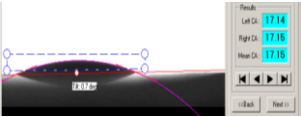
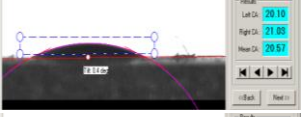

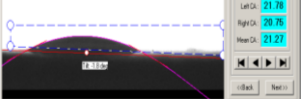


Fig. 6.2. FT-IR spectra of nanostructured samples incorporating amoxicillin.

VI.3.3. Surface wettability analysis

The contact angles values for water drops deposited on the nanostructured surfaces are presented in Table 6.2. All modified samples with amoxicillin have a contact angle value between 17° to 21°, being largely in agreement with the findings of other investigations [3]. There is not a visible difference in the wettability of these samples, all of them possessing a powerful hydrophilic character. This might be advantageous for improved cell attachment and proliferation on the surface of implantable materials [8].

Table 6.2. The contact angle of modified surfaces

Samples	Contact angle [°]	Standard deviation [°]
TNT-40V/Amx		±0.52
TNT-80V/Amx		±0.42
TNTr-40V/Amx		±0.45
TNTr-80V/Amx		±0.48

VI.3.4. Electrochemical characterization

VI.3.4.1. Tafel analysis

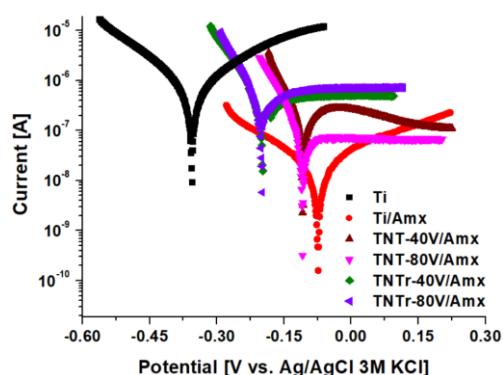


Fig. 6.3. Tafel diagram for the Ti modified samples.

Fig. 6.3 shows the Tafel plots of the modified samples surface. Ti/AMX has the lowest corrosion current and higher electropositive potential comparing to the other samples, thus it is less susceptible to corrosion.

The corrosion parameters were calculated using NOVA software by extrapolating the both cathodic and anodic curves (Table 6.3).

Table 6.3. The principal corrosion parameters

Samples	Corrosion potential [V]	Corrosion current density [A/cm ²]	Corrosion rate [mm/year]
Ti	-0.35	$9.58 \cdot 10^{-7}$	$111 \cdot 10^{-4}$
Ti/Amx	-0.08	$2.50 \cdot 10^{-7}$	$18.32 \cdot 10^{-4}$
NT-40V/Amx	-0.10	$4.58 \cdot 10^{-7}$	$53.28 \cdot 10^{-4}$
NT-80V/Amx	-0.11	$3.26 \cdot 10^{-7}$	$37.87 \cdot 10^{-4}$
TNTr-40V/Amx	-0.20	$6.47 \cdot 10^{-7}$	$75.22 \cdot 10^{-4}$
TNTr-80V/Amx	-0.20	$7.16 \cdot 10^{-7}$	$84.80 \cdot 10^{-4}$

The Ti/Amx sample is the most stable in terms of corrosion, having the lowest corrosion rate when compared to the other samples. According to our investigations, Amx represents a protective layer for the Ti surface, reducing the corrosion rate for Ti/Amx compared to the Ti sample [3].

The corrosion rate and corrosion current densities increased slightly when Amx was loaded into the nanotubes substrate, most likely because of the interaction between Amx and these nanostructures. However, as compared to titanium substrate, the corrosion rate is significantly reduced for all modified samples.

VI.3.4.2. Spectroscopie electrochimică de impedanță

Fig. 6.4 shows the Nyquist plots correlating with the analysed samples. As a first observation, from EIS analysis: all modified samples have higher resistance than untreated Ti, being more stable.

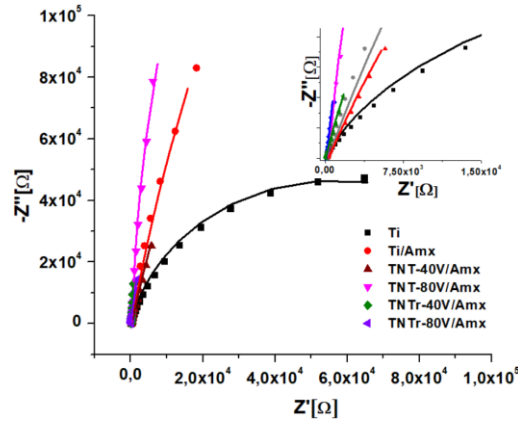


Fig. 6.4. Nyquist diagrams of modified samples, performed in NaCl (aq).

The circuit parameters, obtained using the Nova software, are presented in Table 5. Taking into account the similarity of the electrolyte and test conditions, the solution resistance is practically identical for all examined samples (approximately 100 Ω). It can be seen that following surface coating, the R_{oxid} increases when compared to titanium substrate. The resistance of the nanotubular layers is higher compared with Ti sample. The deposition of amoxicillin does not bring significant changes in resistance. The native oxide layer's N values for all samples are around 0.9, which suggests a pseudocapacitive behaviour. For the coating layer, N values are smaller than 0.5 indicating pseudo-resistive behaviour.

Table 6.4. Parameters obtained by equivalent circuits

Parameter/ Sample	R_S [Ω]	R_{coating} [Ω]	CPE _{coating}		R_{oxide} [Ω]	CPE _{oxide}		X^2
			Y_0 [S^*s^N]	N		Y_0 [S^*s^N]	N	
Ti	75.5	-	-	-	$0.11 \cdot 10^6$	$2.60 \cdot 10^{-5}$	0.87	0.07
Ti/Amx	97.8	$2.0 \cdot 10^2$	$0.80 \cdot 10^{-3}$	0.43	$1.10 \cdot 10^6$	$1.83 \cdot 10^{-5}$	0.91	0.06
TNT-40V/Amx	99	$7.0 \cdot 10^2$	$2.31 \cdot 10^{-3}$	0.45	$0.87 \cdot 10^6$	$19.31 \cdot 10^{-5}$	0.89	0.23
TNT-80V/Amx	89	$9.0 \cdot 10^2$	$1.45 \cdot 10^{-3}$	0.47	$1.11 \cdot 10^6$	$18.64 \cdot 10^{-5}$	0.99	0.21
TNTr-40V/Amx	96.8	$9.1 \cdot 10^2$	$31.40 \cdot 10^{-3}$	0.39	$2.00 \cdot 10^6$	$0.11 \cdot 10^{-5}$	0.97	0.01
TNTr-80V/Amx	74.5	$9.0 \cdot 10^2$	$11.01 \cdot 10^{-3}$	0.47	$0.62 \cdot 10^6$	$9.12 \cdot 10^{-5}$	0.94	0.01

VI.3.4.3. Cyclic voltammetry

It can be seen from table 6.5 that the value of C_{dl} increases from 0.23 to 0.3 mF/cm^2 , for the samples having the Ti surface modification with amoxicillin. This behaviour is in agreement with the findings of our investigations [3]. The development of nanotubular structures on the titanium surface improve the surface's hydrophilicity, accelerating charge transfer at the interface and the production of electric double layers and thus the electrochemical capacitance of the porous structures of nanotubular samples which is significantly influenced by ion diffusion and charge transfer could be amplified

The studied samples had high C_{dl} values, particularly the samples based reduced nanotubes (TNTr_40V/Amx = 1,74 mF/cm^2 și TNTr_80V/Amx = 1,58 mF/cm^2). This may indicate a more effective ion absorption/desorption process at the interface between the electrolyte solution and nanostructured surface.

Table 6.5. C_{dl} values calculated from CV diagrams for tested samples

Sample	C_{dl} [mF/cm^2]
Ti	0.23
Ti/Amx	0.30
TNT-40V/Amx	0.81
TNT-80V/Amx	0.84
TNTr-40V/Amx	1.74
TNTr-80V/Amx	1.58

VI.3.5. 4. *In vitro* amoxicillin release

All nanostructured samples studied incorporated approximately the same amount of amoxicillin (60%), probably due to a better interaction between Amx and TiO₂ nanotubes (Fig.6.7).

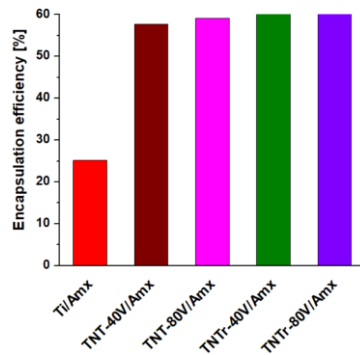


Fig. 6.7. The amoxicillin encapsulation efficiency.

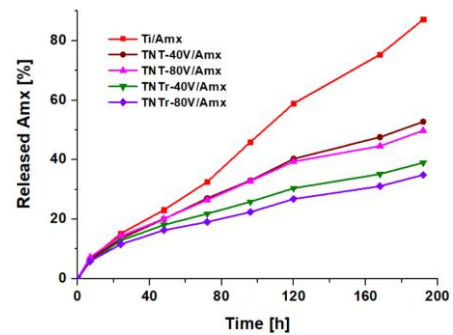


Fig. 6.8. AMX release in phosphate buffer

The amoxicillin release curves of all the samples over 192 hours are seen in Fig. 6.8. There were not substantial changes in the first 120 hours between the TNT-40V/Amx and TNT-80V/Amx samples, the release of Amx being 40.32% and 39.38% respectively. In the case of the TNTr-80V/Amx, sample, was observed the slowest quantity of Amx released, at 26.82%. After 192 h, a drug release of 87.12% (Ti/Amx), 52.78% (TNT-40V/Amx), 49.81% (TNT-80V/Amx), 39.01% (TNTr-40V/Amx) and 34.92% (TNTr-80V/Amx)

Compared to the TNT-40V and TNT-80V substrates, the slower release may be achieved while using reduced nanotubes (TNTr-40V și TNTr-80V).

The distinct morphology of the TiO₂ nanotubes produced after anodizing can be used to explain this behaviour. The release is similar in the first hours because the antibiotic is released from the upper part of the nanotubes.

According to our investigations, Amx can be fixed on the nanostructured Ti surface using either TNT or TNTr. In addition, TNTr demonstrates improved performance in terms of time-release of amoxicillin, making these materials suitable for topical drug delivery applications.

CHAPTER VII. MODIFICATION OF TI IMPLANTS SURFACES WITH TiO₂ NANOTUBES/ SILK FIBROIN /nZNO FOR ENHANCED ANTIMICROBIAL EFFECT

Considering the notions presented above, the present work proposes a novel ap-proach in creating Ti coatings with improved antimicrobial effect, using nature-inspired biomimetic polymers. Firstly, the surface of Ti was nanostructured with TiO₂ nanotubes, followed by the deposition of silk fibroin fibers, using an electrospun process. An important aspect of originality for this work consists in approaching and optimizing different methods for coating functionalization process with ZnO, as antibacterial agent. This was achieved using three methods and the resulting hybrid coating properties were evaluated comparatively to assess the morphology, topography, wettability, and antibacterial effect properties that will determine the biological behavior of the material. Furthermore, electrochemical stability, an issue not very often addressed in literature for these types of coatings, was discussed in correlation with the chemical structure.

VII.3. SURFACE CHARACTERIZATION

VII.3.1. Surfaces morphology and composition

The SEM results of the nanostructured titanium demonstrated that the surface is covered with nanotube structures with uniform morphology and neat arrangement. Top view and cross-section SEM images of the sample obtained by anodizing in aqueous $\text{NH}_4\text{F}/\text{H}_2\text{O}/\text{EG}$ electrolyte are presented in Figure 1. In these experimental conditions, self-organized and vertically aligned nanotubes grew at the surface of Ti. In addition, the nanotubes are well-defined and uniformly distributed across the surface with an open-top morphology without the presence of nanograss, as seen in Fig. 7.1a. They have external diameters of around 90 nm and thin walls (Fig. 7.1b). The cross-section images (Fig. 7.1c) showed nanotubes length around 7.5 μm . It is visible that nanotubes have a bamboo-like structure on the exterior.

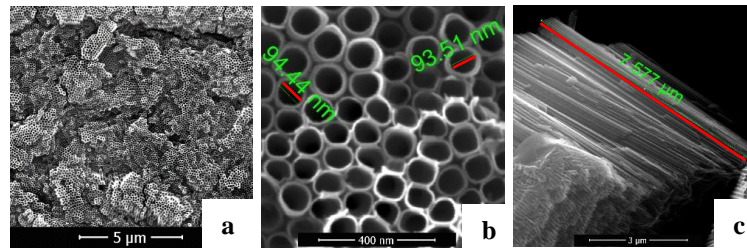


Fig. 7.1 SEM images : a) represents TNT-40V sample, b) represents the top view of TNT-40V sample and c) represents the cross-section

Fig. 7.2 shows the morphology of electrospun SF fibers before and after immobilization of ZnO NPs on the TiO_2 nanotubes surface, as well as the EDX spectra for samples containing ZnO. Fig. 7.2a shows a dense layer of interconnected smooth silk fibroin fibers in a wide range of thicknesses and lengths. High magnification revealed a diameter of 326 nm for SF fibers. The fibers were uniformly spread on top of nanotubes, resulting in a matrix that combines the microstructure of SF fibers and the nanostructure corresponding to TiO_2 nanotubes. This is an important aspect because the modified surface did not have the same morphology, which is good for the cell's attachment. Fig. 7.2b și 7.2c indicate that the ZnO nanoparticles addition has no impact on the SF fibers morphology. The size of SF fibers changed after polydopamine immobilization, becoming coarser ($d = 450 \text{ nm}$; Fig. 7.2d). Small aggregates were deposited on the fiber surface following ZnO coating, as illustrated in Fig. 7.2d.

The results of EDX study of the TNT/SFef-nZnO, TNT/nZnO/SFef and TNT/SFef/PD/nZnO samples are shown in Fig. 7.2e, 7.2f și 7.2g. Zinc, oxygen and titanium peaks have been identified. Zn percentage in all the three samples is comprised between 0.37 – 0.47. This indicates that nZnO were successfully embedded into the hybrid matrix.

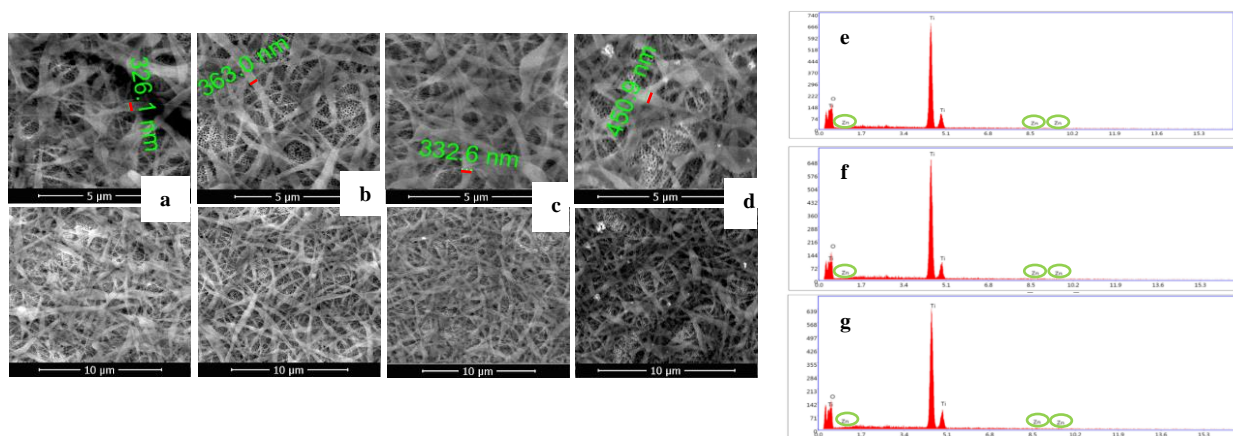
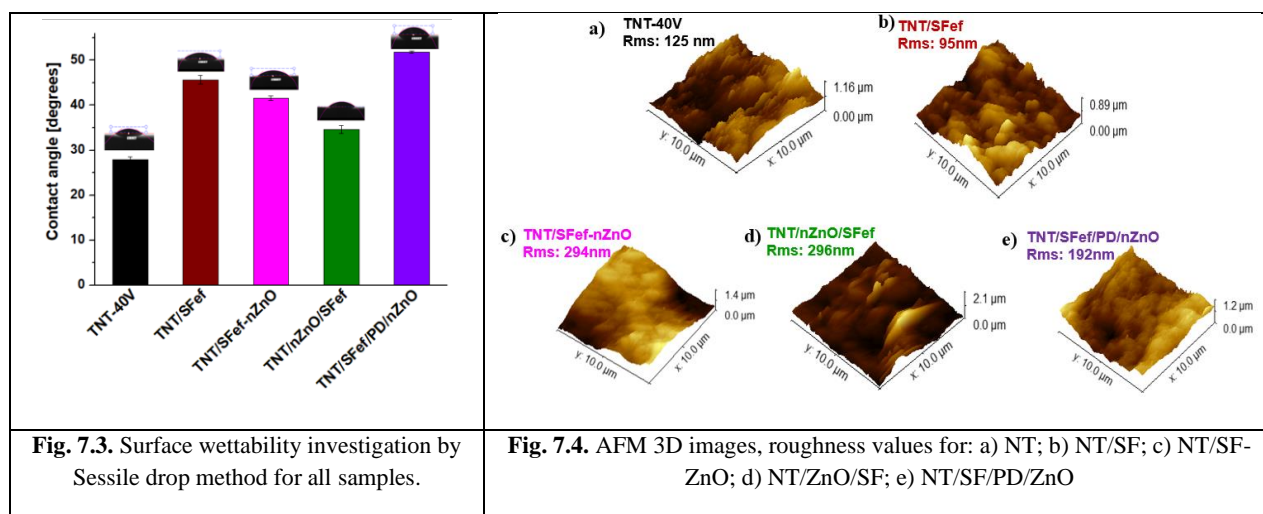


Fig. 7.2. SEM images corresponding to a) TNT/SFef; b) TNT/SFef-nZnO; c) TNT/nZnO/SFef; d) TNT/SFef/PD/nZnO and corresponding EDX diagrams for ZnO containing samples: e) TNT/SFef-nZnO, f) TNT/nZnO/SFef și g) TNT/SFef/PD/nZnO

SEM analysis reveals that all samples present a uniform distribution of TiO_2 nanotubes and SF nanofibers. Therefore, EDX analysis demonstrates the presence of Zn nanoparticles on the modified TNT-40V surface.

VII.3.2. Surface topography and wettability

In this study, Sessile drop method was utilized to investigate the influence of chemical composition of the coatings and roughness on the wettability of nanotubular surfaces (Fig. 7.3). The contact angles of TNT-40V and TNT-SFef surfaces were measured as $28^\circ \pm 0.57^\circ$ and $46^\circ \pm 0.99^\circ$ respectively, as was also observed in our previous research [4]. It is obvious that all surfaces have hydrophilic character because the contact angle is $< 90^\circ$. The hydrophilicity of the nanotubular surface decreases when SF fibers are deposited (Fig. 7.3). This decrease is explained based on the presence of hydrophobic domains in SF as well as its β -sheet crystal structure [32]. With the addition of ZnO, the contact angle reduced to $42^\circ \pm 0.51^\circ$ in TNT/SFef-nZnO and $35^\circ \pm 0.9^\circ$ in TNT/nZnO/SFef. The contact angle corresponding to TNT/SFef/PD/nZnO has a value of $52^\circ \pm 0.28^\circ$ and is very comparable to the PD substrate that was previously published [4].



Bone-implant interface development and bacterial contact are both highly dependent on surface roughness [33, 34].

Fig. 7.4 presents 3D AFM images corresponding to all tested samples. The roughness of the TNT/SFef sample decreased to 95 nm from 125 nm that correspond to the TNT-40V substrate, while the contact angle increased. The roughness and hydrophilicity of the samples containing SF and ZnO nanoparticles (TNT/nZnO/SFef și TNT/SFef-nZnO) are higher than those of TNT/SFef. Correlating this with wettability, Wenzel model can be applied: by increasing the surface roughness, the hydrophilic substrate becomes more hydrophilic [35-37].

Compared with the TNT/SFef substrate, the TNT/SFef/PD/nZnO sample has a higher roughness and contact angle. This “mushroom state”, kind of wetting behavior, is an intermediate state between the Cassie-Baxter and Wenzel models [3].

The variety of morphologies might be used to explain these differences in water contact angle. Hydrophilic surfaces generally exhibit resistance to microbial adhesion, hence preserving their cleanliness. Investigation has demonstrated that biomaterials exhibiting higher levels of hydrophilicity facilitate enhanced cellular connections [38].

VII.3.3. FT-IR analysis

In the case of this study the amide I, II, and III peaks at 1614 , 1520 , 1445 , and 1230 cm^{-1} were attributed to the obtained 6.45 % silk fibroin solution (Fig. 7.5). The peaks for the TNT/SFef, TNT/SFef-nZnO and TNT/nZnO/SFef samples had about the same values, indicating that the nanostructured surface was effectively coated with fibroin. The characteristic peaks at 1623 cm^{-1} , 1520 cm^{-1} , and 1225 cm^{-1} indicate that silk fibroin is in a β -sheet conformation. The presence of ZnO nanoparticles does not influence the FTIR spectrum.

According to our results [3], polydopamine has peaks at 3350 cm^{-1} (OH and NH stretches), 1283 and 1631 cm^{-1} (stretching vibration of catechol hydroxyl C-O and C=O), and 1523 cm^{-1} (C = C bonds in the indole structure). Because

PD and SF are natural polymers, their peaks are comparable (1631 and 1523 cm^{-1}). Consequently, there are no significant changes in the FTIR peak between the TNT/SFef and TNT/SFef/PD/nZnO samples, indicating that both polymers were deposited on the nanotubular surface.

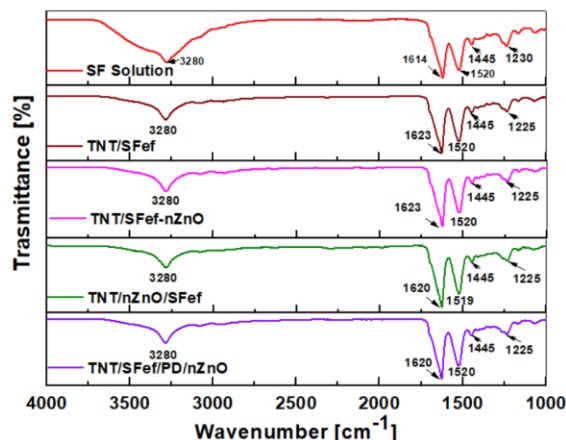


Fig. 7.5. FT-IR images corresponding to the studied samples.

VII.3.4. Electrochemical characterization

VII.3.4.1. Electrochemical impedance spectroscopy

It can be observed from data presented in Table 7.2 the values for R_{sol} are similar, for all tasted samples and have values between 60 and 100, the same electrolyte solution being used for all tests. Compared to the pristine TNT-40V surfaces, the modified TNT-40V surfaces possess a higher re-sistance of the compact oxide layer (R_{oxide}). These values demonstrate an excellent relationship with the Tafel diagram results, which show that the corrosion rates of the modified TNT-40V samples were lower than those of the pristine TNT-40V sample.

When ZnO nanoparticles are added (TNT/nZnO/SFef și TNT/SFef-nZnO), the barrier oxide layer's resistance increases compared to the TNT/SFef sample. In other study, the resistance value of pure TiO_2 nanostructures arrays decreased after direct modification with ZnO by hydrothermal method [39]. In our study, the second resistance associated with the coating ($R_{coating}$) is higher for all modified TNT-40V samples compared to the pristine NT substrate. A possible explanation could be that SF and ZnO nanoparticles are deposited at the surface of the nanotubes layer. Moreover, it can be observed that the TNT/SFef-nZnO and TNT/nZnO/SFef samples presented higher coating resistances than the TNT/SFef substrate, being more stable.

TNT/SFef/PD/nZnO has a smaller semicircle diameter in Nyquist plot compared to other modified TNT-40V samples. This suggests a reduced charge transfer resistance and a significantly increased charge transport at the electrode/electrolyte contact [40]. Most samples have N values for the oxide layer and surface coating in the range of 0.61 to 0.98, indicating pseudocapacitive behavior.

Table 7.2. Values obtained from fitted EIS data using NOVA software.

Parameters Samples	R_s [Ω]	R_{PD} [Ω]	CPE_{PD}		$R_{coating}$ [Ω]	$CPE_{coating}$		R_{oxide} [Ω]	CPE_{oxide}		X^2
			Y_0 [$\mu\text{S}\cdot\text{s}^n$]	N		Y_0 [$\mu\text{S}\cdot\text{s}^n$]	N		Y_0 [$\mu\text{S}\cdot\text{s}^n$]	N	
NT	99	-	-	-	$4\cdot 10^3$	62	0.71	$20\cdot 10^3$	149	0.68	0.01
NT/SF	91	-	-	-	$8\cdot 10^3$	266	0.92	$136\cdot 10^3$	65	0.96	0.07
NT/SF-ZnO	68	-	-	-	$9\cdot 10^3$	278	0.82	$156\cdot 10^3$	900	0.93	0.04
NT/ZnO/SF	68	-	-	-	$10\cdot 10^3$	356	0.87	$184\cdot 10^3$	897	0.98	0.03
NT/SF/PD/ZnO	63	$1.7\cdot 10^3$	79	0.74	$5\cdot 10^3$	270	0.61	$92\cdot 10^3$	297	0.89	0.01

The EIS analysis revealed that all modified TNT-40V samples are more stable than the pristine TNT-40V and exhibit pseudo-capacitive behavior.

VII.3.4.2. Tafel analysis

The Tafel diagrams (Fig. 7.7) were used to obtain the electrochemical parameters for the investigated surfaces: corrosion potential (E_{corr}), corrosion current (i_{corr}), and corrosion rate (v_{corr}).

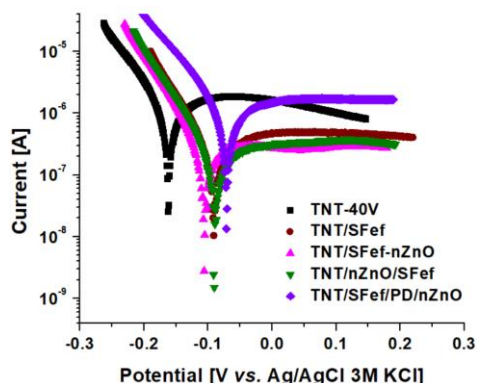


Fig. 7.7. Tafel diagram for the studied samples, recorded in NaCl 0.9%.

Figure 7.7 demonstrates how similar all the polarization curves were to one another. This implied that all the TNT/SFef-nZnO, TNT/nZnO/SFef, TNT/SFef/PD/nZnO composite coatings in this investigation used a similar polarization mechanism. The corrosion parameters were obtained by extrapolating the anodic and cathodic curves (Table 7.3). In addition, the protection effectiveness was calculated using the formula [65].

Table 7.3. Corrosion parameters for studied samples.

Samples	Corrosion potential [V]	Corrosion current density [A/cm^2]	Corrosion rate [mm/year]	Protection efficiency [%]
TNT-40V	-0.161	$3.896 \cdot 10^{-6}$	0.0452	-
TNT/SFef	-0.092	$0.359 \cdot 10^{-6}$	0.0042	91
TNT/SFef-nZnO	-0.104	$0.249 \cdot 10^{-6}$	0.0029	94
TNT/nZnO/SFef	-0.091	$0.119 \cdot 10^{-6}$	0.0014	97
TNT/SFef/PD/nZnO	-0.071	$0.568 \cdot 10^{-6}$	0.0066	84

In general, a material with a lower corrosion current density and a higher corrosion potential has a reduced propensity to corrode and hence performs better against corrosion [41].

The corrosion potential was moved to positive values for TNT/SFef and all modified ZnO samples compared to pristine TNT-40V as may be shown in Table 7.3. It is evident that the surface modification with silk fibroin caused a decrease of corrosion potential from -0.161 V for TNT-40V to more electropositive values, up to -0.071 V for TNT/SFef/PD/nZnO, demonstrating an increase in TNT-40V surface stability following the coating deposition. Similarly, the density of corrosion currents was found to be lower for coated samples compared to TNT-40V, suggested the same thing. Therefore, the corrosion current density decreased from $3.89 \cdot 10^{-6} A/cm^2$ for TNT-40V to values 6–9 times lower for modified samples.

Compared to pristine TNT-40V, all modified samples containing silk fibroin and ZnO nanoparticles exhibit better electropositive potentials. The samples TNT/nZnO/SFef and TNT/SFef-nZnO exhibit decreased susceptibility to corrosion than TNT-40V samples due to lower corrosion currents. The TNT/nZnO/SFef sample showed a lower corrosion rate (0.0014 mm/year) compared to TNT-40V (0.452 mm/year).

TNT/nZnO/SFef presents the highest corrosion protection efficiency (97 %). Probably the ZnO nanoparticles deposited on nanotube walls can passivate the TiO_2 surface defect states.

All coatings contributed to increased corrosion stability and highest corrosion protection efficiency compared to pristine TNT-40V.

VII.3.4.3. Cyclic voltammetry

The double-layer capacitance (C_{dl}) may be a fundamental structural characteristic for surface interactions, being determined by the relationship between the surface charge and the oxide-solution interface [3, 42].

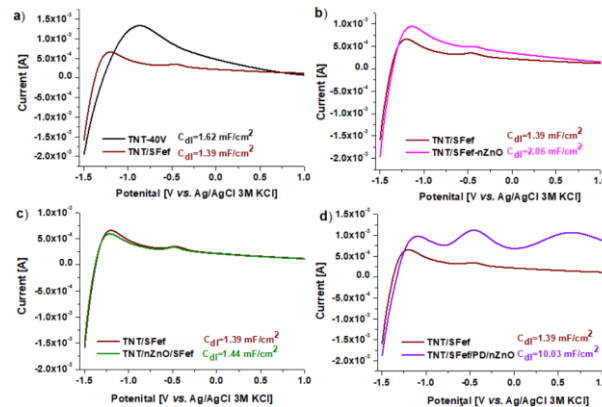


Fig. 7.8. Ramura anodică a voltamogramelor ciclice pentru toate probele testate, utilizate pentru calculul C_{dl} .

The titania nanotubes electrodes' regular pore size and hollow tube morphology make it simple to transfer charges and boost interfacial ion movement, which leads to improved capacitive performance [43]. In the nanotube layer, the open pore mouth structure helps make electrolyte ion diffusion possible [44]. The growth of the silk fibroin layer on the TNT-40V surface led to the smoothing of the surface, as observed in AFM analysis and the covering of some nanotubes as seen from SEM images. Thus, the active surface area decreases, and the double layer capacity is reduced for TNT/SF_{ef} compared with TNT-40V (Fig. 7.8a).

By nZnO depositing on the TNT/SF_{ef} substrate, Fig. 7.8b-c the sample surface determines an increase of the active surface and Faradaic current, as well as C_{dl} (from 1.39 to 2.06 or 1.44 mF/cm²). Thus, TNT/SF_{ef} surface modification with ZnO nanoparticles improved the surface's hydrophilicity, wettability, and roughness, thus speeding up the rate of charge transfer at the interface and the electrical double layers formation. The porous structure of both TNT/nZnO/SF_{ef} and TNT/SF_{ef}-nZnO can be especially attributed to charge transfer and ion diffusion, which have a significant impact on its electrochemical capacitance. The TNT/SF_{ef}/PD/nZnO sample has the highest C_{dl} value (10.03 mF/cm²), efficient ion absorption/desorption process at the interface between this surface and the electrolyte solution. The C_{dl} value obtained for TNT/SF_{ef}/PD/nZnO sample is comparable to the values obtained for TiO₂ nanotubes boron-doped diamond nanostructures from other studies [45].

VII.3.5. *In vitro* antibacterial assay

To evaluate the antibacterial activity of the newly created surfaces, the following human pathogenic microbial strains were investigated: *Staphylococcus aureus* and *Enterococcus faecalis*.

It is already known from literature that nano-structuring the titanium surface with nanotubes leads to a slight increase in inhibition of growth compared with pristine titanium because the great hydrophilicity of the nanotubes and the modest number of negative charges on the surface may help to hinder the attachment of bacteria through the property of non-specific protein adsorption [46]. Thus, the importance of surface morphology could be already highlighted with this first level of surface modification. Herein, TNT-40V sample is used as reference to report the results for the hybrid films.

When the TiO₂ nanostructures are covered with SF fibers, the inhibition of growth continued to slightly increase for both tested bacteria. Although from literature it is already known that SF lacks the antimicrobial property in our study an supplementary inhibition of growth was obtained for TNT/SF_{ef} coated samples. Compared to TNT-40V,

sample, the surface roughness didn't vary, only the wettability decreased. Thus, this change could be associated to the surface chemistry, due to the interaction between charged functional groups of silk fibroin and the bacterial cell surface.

The presence of encapsulated ZnO nanoparticles lead to an inhibition of growth that increased considerably. For the case when nZnO was fixed on the TNT-40V nanotubes before SF deposition, the results for antimicrobial test are very comparable with the situation when the functionalization of the coating with ZnO is made at the same time with SF electrospun. The ZnO nanoparticles and the bacterium have opposite charges, which results in electrostatic forces that firmly adhere the nanoparticles to the bacteria's surface and harm the cell membrane [47].

An interesting observation is that in the case of using polydopamine as intermediate layer for embedding ZnO, the inhibition of growth was higher, up to 55 % and 53 % respectively, for both microorganisms. This was an expected difference considering the following aspects: 1) the percentage of Zn is superior comparing to the other two coatings 2) the presence of polydopamine change the surface properties in a more pronounced manner: the surface chemistry, topography, and wettability. Thus, this result is probably a cumulative effect.

Table 7.4. Antibacterial effect for the modified Ti surfaces with NT, SF and ZnO.

Samples	<i>Enterococcus faecalis</i>	<i>Staphylococcus aureus</i>
TNT-40V	-	-
TNT/SFef	15	13
TNT/SFef-nZnO	41	39
TNT/nZnO/SFef	42	41
TNT/SFef/PD/nZnO	55	53

This study paves the path for the use of nano-engineered structures (nanotubes) together with the natural, non-toxic features of silk fibroin and dopamine polymers in anti-corrosion and antibacterial nanocomposite coatings for titanium metallic implants surface modification.

CHAPTER VIII. HYBRID TITANIUM SURFACE COVERING WITH REDUCED TiO₂ NANOTUBES/ SILK FIBROIN/ NZNO FOR ENHANCED ANTIBACTERIAL EFFECT

Considering all theoretical aspects already discussed, in the present study, TNTr2 surfaces were obtained, optimized and compared with TNT-40V in terms of surface properties. The selected Ti nanostructured surfaces were subjected to silk fibroin deposition using electrochemical technique, an issue not often addressed in literature. Then, a novel hybrid coating was obtained by film functionalization with therapeutically ZnO nanoparticles as an antibacterial agent. The antibacterial effect was evaluated against *S. aureus* and *E. coli*, highlighting the correlation between the surface properties of modified and non-modified TNTr2 surfaces and antibacterial activity.

VIII.3.1. SF and SF-ZnO electrodeposition

Biomimetic fibroin coatings were obtained using the electrodeposition on the Ti modified surfaces, an approach that is not often addressed in literature, about fibroin processing.

VIII.3.2. Morphology and composition of modified surfaces

The nanostructured titanium surfaces electrochemically coated with fibroin films with or without ZnO nanoparticles were morphological analyzed through SEM analysis . These films were deposited over the TiO₂ nanotubes in the form of microporous structure, with the pore diameters of several hundred nanometers.

VIII.3.3. FT-IR analysis

Interactions between SF and TNT-40V surface were detected by FTIR spectroscopy. Different crystalline SF forms have been shown to display absorption bands in different vibrational areas linked to the protein's amide groups [48, 49]. All TNT-40V and TNTr2 samples modified with SF or SF-nZnO show peaks similar to silk fibroin solution. This confirms that SF was effectively attached to the surfaces of TiO₂ nanotubes.

VIII.3.4. Wettability and surface topography

For titanium dioxide nanotubes (TNT-40V și TNTr2) the contact angle was approximately 30°, indicating a hydrophilic surface, as already observed in another previous study [4, 50]. Deposition of the fibroin coating leads to a higher contact angle values that are induced by the hydrophobic regions of the fibroin structure (crystalline sheets) formed after methanol treatment, as already reported [3, 4]. However, the samples have contact angle values less than 65°, indicating that they still have a weak hydrophilic character.

VIII.3.5. Electrochemical characterization

VIII.3.5.1. Tafel analysis

Tafel plots are shown in Fig. 8.5. All modified samples with nanotubes and silk fibroin, with or without ZnO nanoparticles, have more electropositive potentials than the Ti substrate modified with TNT-40V and TNTr2. The samples TNT/SFech and TNT/SFech-nZnO have lower corrosion currents than TNT-40V samples, thus proving a less susceptible character for corrosion.

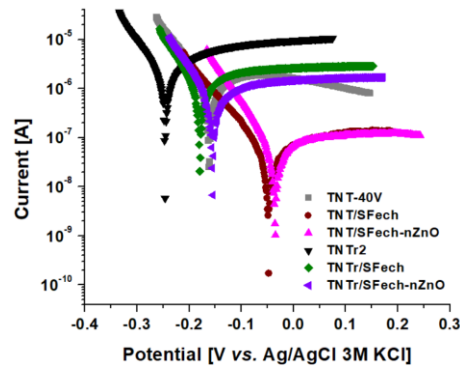


Fig. 8.5. Diagrama Tafel pentru probele de Ti modificate.

By extrapolating anodic and cathodic curves, there were obtained the corrosion parameters (Tabelul 8.2).

VIII.3.5.2. Impedance spectroscopy

In Fig. 8.6a are presented Nyquist diagram corresponding to the coated surface samples. As a first observation, all modified surfaces have higher resistance and are more stable comparing with TNT-40V samples.

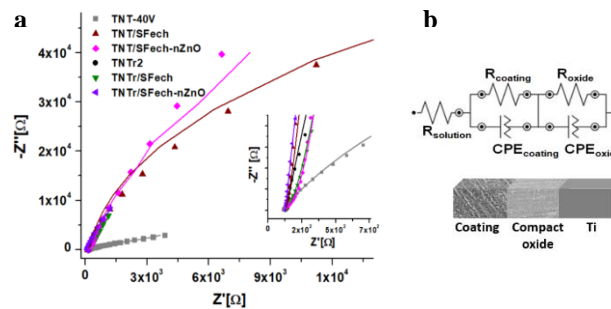


Fig. 8.6. a) Impedance diagram for modified samples and b) Circuits used to fit EIS data for coated samples.

VIII.3.6. In vitro antibacterial assay

Two different types of pathogenic bacteria were used for the antibacterial study: *E. Coli* (gram negative) and *S. aureus* (gram positive).

Table 8.5. Values obtained for CFU, antibacterial effects and susceptibility constants.

Samples	CFU		R		Z value	
	[CFU/mL]		[%]		[mL/ μ g]	
	<i>E. coli</i>	<i>S. aureus</i>	<i>E. coli</i>	<i>S. aureus</i>	<i>E. coli</i>	<i>S. aureus</i>
Ti	648	770	C*	C		
TNT-40V	578	601	12	21	-	-
TNTr2	472	543	27	29	-	-
TNT/SFech	458	488	29	36	-	-
TNTr/SFech	354	441	45	43	-	-
TNT/SFech-nZnO	255	275	61	64	0.01	0.009
TNTr/SFech-nZnO	165	203	75	74	0.013	0.012

*C - Control

As can be seen, the antibacterial activity increases with changes to the surface's chemistry, morphology, roughness, wettability, surface energy, surface charge, and presence of zinc oxide.

In conclusion, the antibacterial effect tested against *S. aureus* and *E. coli* emphasizes the value of surface properties, including (I) surface morphology after nanotube growth, (II) surface conductivity and band gap energy after TiO₂ nanotube reduction, (III) improvement of the surface's visible light absorption by SF deposition, and (IV) surface charge and Zn²⁺ ions delivery after ZnO incorporation.

This study created a new biomimetic hybrid coating with improved antibacterial properties for titanium implants by combining a nanostructured reduced TiO₂ nanotubes and a silk fibroin biopolymer encapsulating therapeutically ZnO nanoparticles.

CHAPTER IX. CONCLUSIONS AND FUTURE PERSPECTIVES

IX.1. GENERAL CONCLUSIONS

This work aims to modify implantable titanium surfaces, used in biomedical applications, such as replacing or supporting bone tissue. In order to improve osseointegration, the titanium surface was modified with TiO₂ nanostructures and natural polymers. In their presence, the incorporation of materials with an antibacterial effect (amoxicillin, ZnO nanoparticles) was achieved, for their local release. These are used in the medical industry, in particular, to prevent bacterial infections.

Initially, the titanium surface was modified with two biopolymers, polydopamine and silk fibroin, by self-polymerization and electrodeposition, respectively. They were used as intermediate organic films, for better binding of amoxicillin.

- The SEM images demonstrated that amoxicillin was well bound on the titanium surface by means of the two biopolymers. FTIR analysis revealed stronger π - π interactions and hydrogen bonds between PD and Amx and possible spontaneous conjugation of silk protein with Amx.
- Improved stability of all titanium modified samples was also highlighted, revealing better behavior of SF modified sample.
- Release studies showed that fibroin and polydopamine can graft amoxicillin to the Ti surface and release it, according to the Korsmeyer-Peppas model. By loading amoxicillin through polydopamine, the antibiotic can be released slowly over a longer period of time.
- Antibacterial studies against *E. coli*, *S. mutans* and *L. fermentum* have shown that this binding method allows the antibacterial effect of amoxicillin to be preserved for a long time. Ti/PD/Amx leads to the highest inhibition effect against all three microorganisms tested.

Subsequently, the Ti surfaces were modified with unreduced and reduced TiO₂ nanotubular structures through an anodization process using different parameters. Selected nanostructured Ti samples were functionalized with an

active compound, Amoxicillin. Amx-modified surfaces were characterized in terms of morphology, wettability, electrochemical stability and antibiotic release.

- SEM analysis demonstrated that the surface of the Ti samples was completely covered with self-organized nanotubes, with uniform diameters. FTIR analysis indicated that Amx was loaded onto the nanostructured surfaces.
- All samples with modified surfaces have better electrochemical stability compared to untreated titanium.
- According to this investigation, Amx can be fixed on Ti surface using unreduced and reduced TiO₂ nanotubes. TNTr demonstrated improved performance in amoxicillin release over time. This lucu makes these materials suitable for topical drug delivery applications.

Also, nanostructured TiO₂ surfaces were coated with SF/nZnO, by electrospinning, using different methods to incorporate ZnO nanoparticles into the hybrid film.

- According to SEM examination, TNTs presented a uniform morphology and arrangement, with thin walls and outer diameters of about 90 nm. Silk fibroin nanofibers were uniformly distributed on the nanotubular surfaces.
- FT-IR spectra showed characteristic peaks, which demonstrate that the nanostructured surface was effectively coated with fibroin. EDX analysis proved the presence of ZnO nanoparticles on the SF-modified TNT surface.
- All the modified samples presented a hydrophilic character.
- According to electrochemical tests, all modified TNT samples have a pseudocapacitive character and are more stable than untreated TNT, having a high level of corrosion protection (over 80%).
- In vitro antibacterial effect was tested against *E. faecalis* and *S. aureus*. Encapsulated ZnO nanoparticles caused a growth inhibition that was much more pronounced. Growth inhibition was higher for both microorganisms when polydopamine was used as an interlayer for ZnO incorporation, reaching up to 55% against *E. faecalis* and 53% against *S. aureus*.

Finally, unreduced and reduced TiO₂ nanotube-modified titanium surfaces were coated with SF/ZnO by electrochemical method. Silk fibroin, a biomimetic polymer obtained from *Bombyx Mori* cocoons, was used as a matrix to incorporate ZnO nanoparticles.

- SEM analysis showed that silk fibroin was deposited over TiO₂ nanotubes in the form of a microporous structure, with pore diameters of several hundred nanometers.
- FT-IR spectra showed characteristic peaks, which demonstrate that the nanostructured surface was effectively coated with silk fibroin. EDX analysis proved the presence of zinc oxide on the nanostructured surfaces.
- Electrochemical results show better surface conductivity and lower bandgap energy for TNTr surfaces compared to TNT, which could be advantageous for improving antimicrobial surface activity.
- The antibacterial effect evaluated against *S. aureus* and *E. coli* highlights the importance of surface properties: (i) surface morphology after nanotube growth, (ii) surface conductivity and band gap energy after TiO₂ nanotube reduction, (iii) improvement of surface visible light absorption by SF deposition and (iv) surface charge and release of Zn²⁺ ions after nZnO incorporation. All these properties determine an improved antibacterial effect.

This study opens the perspective of using nanoengineered structures (nanotubes) together with the natural, non-toxic characteristics of polymers, silk fibroin and dopamine, in anticorrosive and antibacterial nanocomposite coatings for surface modification of titanium metal implants.

IX.2. FUTURE PROSPECTSE

- For all modified titanium surfaces, further studies of the interactions with human cells are needed to obtain detailed information about the biocompatibility of these new surfaces..
- For the samples with reduced TiO₂ nanotubes, electrical stimulation tests will be done to see if the surface conductivity influences the release of therapeutic agents, respectively the increase of osseointegration.
- Release studies will be done for samples containing ZnO nanoparticles.
- Electrochemical stability testing will be carried out, respectively that of the antibacterial activity for a longer time.

Selective Bibliography:

- [1]. C. Dumitriu, M. Popescu, G. Voicu, I. Demetrescu. Influence of Anodizing Potential on Titanium Dioxide Nanotubes Morphology. *REVISTA DE CHIMIE*. 2013;64(6):599-602.
- [2]. A.G. PĂUN. TiO₂ SURFACES MODIFICATION FOR AMOXICILLIN RELEASE USED IN DENTAL IMPLANTOLOGY.
- [3]. A.G. Olaru, V. Butculescu, C. Dumitriu, N. Badea, S. Popescu, C. Ungureanu, C. Pirvu. Biopolymers as intermediate layers for amoxicillin grafting on antibacterial surface. *Surfaces and Interfaces*. 2022;33:102224.
- [4]. S. Popescu, M.-E. Zarif, C. Dumitriu, C. Ungureanu, C. Pirvu. Silk Fibroin-Based Hybrid Nanostructured Coatings for Titanium Implantable Surfaces Modification. *Coatings*. 2020;10(6):518.
- [5]. S. He, P. Zhou, L. Wang, X. Xiong, Y. Zhang, Y. Deng, S. Wei. Antibiotic-decorated titanium with enhanced antibacterial activity through adhesive polydopamine for dental/bone implant. *Journal of The Royal Society Interface*. 2014;11(95):20140169.
- [6]. C. Ungureanu, C. Dumitriu, S. Popescu, M. Enculescu, V. Tofan, M. Popescu, C. Pirvu. Enhancing antimicrobial activity of TiO₂/Ti by torularhodin bioinspired surface modification. *Bioelectrochemistry*. 2016;107:14-24.
- [7]. S. Popescu, M.-E. Zarif, C. Dumitriu, C. Ungureanu, C. Pirvu. Silk Fibroin-Based Hybrid Nanostructured Coatings for Titanium Implantable Surfaces Modification. *Coatings*. 2020;10(518).
- [8]. M. Ferrari, F. Cirisano, M.C. Morán. Mammalian Cell Behavior on Hydrophobic Substrates: Influence of Surface Properties. *Colloids and Interfaces*. 2019;3(2):48.
- [9]. V.C. Anitha, J.-H. Lee, J. Lee, A. Narayan Banerjee, S. Woo Joo, B. Ki Min. Biofilm formation on a TiO₂nanotube with controlled pore diameter and surface wettability. *Nanotechnology*. 2015;26(6):065102.
- [10]. M. Padhan, G. Paul, J. Bijwe. Roles of Size, Shape, Amount, and Functionalization of Nanoparticles of Titania in Controlling the Tribo-Performance of UHMWPE Composites. *Frontiers in Materials*. 2020;7.
- [11]. K. Križman, S. Novak, J. Kristl, G. Majdič, N. Drnovšek. Long-acting silk fibroin xerogel delivery systems for controlled release of estradiol. *Journal of Drug Delivery Science and Technology*. 2021;65:102701.
- [12]. N. ul Ain, I. Anis, F. Ahmed, M.R. Shah, S. Parveen, S. Faizi, S. Ahmed. Colorimetric detection of amoxicillin based on querecetagetin coated silver nanoparticles. *Sensors and Actuators B: Chemical*. 2018;265:617-24.
- [13]. E.P. Rebitski, G.P. Souza, S.A.A. Santana, S.B.C. Pergher, A.C.S. Alcântara. Bionanocomposites based on cationic and anionic layered clays as controlled release devices of amoxicillin. *Applied Clay Science*. 2019;173:35-45.
- [14]. S. Sharma, S. Bano, A.S. Ghosh, M. Mandal, H.W. Kim, T. Dey, S.C. Kundu. Silk fibroin nanoparticles support in vitro sustained antibiotic release and osteogenesis on titanium surface. *Nanomedicine*. 2016;12(5):1193-204.
- [15]. H. Luo, C. Gu, W. Zheng, F. Dai, X. Wang, Z. Zheng. Facile synthesis of novel size-controlled antibacterial hybrid spheres using silver nanoparticles loaded with poly-dopamine spheres. *RSC Adv*. 2015;5:13470-7.
- [16]. R. Batul, M. Bhave, P. J. Mahon, A. Yu. Polydopamine Nanosphere with In-Situ Loaded Gentamicin and Its Antimicrobial Activity. *Molecules*. 2020;25(9).
- [17]. C. Fiorica, F.S. Palumbo, G. Pitarresi, G. Biscari, A. Martorana, C. Cala, C.M. Maida, G. Giammona. Ciprofloxacin releasing gellan gum/polydopamine based hydrogels with near infrared activated photothermal properties. *Int J Pharmaceut*. 2021;610.
- [18]. F.E. Ettadili, M. Azriouil, M. Matrouf, F. Laghrib, S. Saqrane, A. Farahi, M. Bakasse, S. Lahrich, M.A.E. Mhammedi. Electrochemical determination of ornidazole at silver electrode: analytical application in human blood. *Chemical Data Collections*. 2022;39:100850.
- [19]. Y. Kadri, E. Srasra, I. Bekri-Abbes, P. Herrasti. Facile and eco-friendly synthesis of polyaniline/ZnO composites for corrosion protection of AA-2024 aluminium alloy. *Journal of Electroanalytical Chemistry*. 2021;893:115335.
- [20]. H.-Y. Wang, Y.-Q. Zhang, Z.-G. Wei. Excess acetone extraction in silk protein solution greatly accelerates the regeneration progress of silk fibroin for desalting and purification. *International Journal of Biological Macromolecules*. 2020;146:588-95.
- [21]. Q. Fu, W. Jin, M. Feng, J. Li, J. Li, W. Li, Z. Yu. An intermediate poly-dopamine layer for alginate coating on high-purity magnesium to achieve corrosion mitigation. *Journal of Magnesium and Alloys*. 2021.
- [22]. M.J. Silvero C, D.M. Rocca, E.A. de la Villarmois, K. Fournier, A.E. Lanterna, M.F. Pérez, M.C. Becerra, J.C. Scaiano. Selective Photoinduced Antibacterial Activity of Amoxicillin-Coated Gold Nanoparticles: From One-Step Synthesis to in Vivo Cytocompatibility. *ACS Omega*. 2018;3(1):1220-30.
- [23]. Y.A. Lee, J. Lee, D.W. Kim, C.Y. Yoo, S.H. Park, J.J. Yoo, S. Kim, B. Kim, W.K. Cho, H. Yoon. Mussel-inspired surface functionalization of porous carbon nanosheets using polydopamine and Fe³⁺/tannic acid layers for high-performance electrochemical capacitors. *Journal of Materials Chemistry A*. 2017;5(48):25368-77.
- [24]. Q. Liu, B. Yu, W. Ye, F. Zhou. Highly selective uptake and release of charged molecules by pH-responsive polydopamine microcapsules. *Macromolecular bioscience*. 2011;11(9):1227-34.

- [25]. J. Yan, D. Xia, W. Zhou, Y. Li, P. Xiong, Q. Li, P. Wang, M. Li, Y. Zheng, Y. Cheng. pH-responsive silk fibroin-based CuO/Ag micro/nano coating endows polyetheretherketone with synergistic antibacterial ability, osteogenesis, and angiogenesis. *Acta Biomater.* 2020;115:220-34.
- [26]. X.Y. Qiao, R. Miller, E. Schneck, K. Sun. Influence of pH on the surface and foaming properties of aqueous silk fibroin solutions. *Soft Matter.* 2020;16(15):3695-704.
- [27]. Y. Ma, B.S.B. Canup, X. Tong, F. Dai, B. Xiao. Multi-Responsive Silk Fibroin-Based Nanoparticles for Drug Delivery. *Front Chem.* 2020;8:585077-.
- [28]. I. Singh, G. Dhawan, S. Gupta, P. Kumar. Recent Advances in a Polydopamine-Mediated Antimicrobial Adhesion System. *Frontiers in Microbiology.* 2021;11.
- [29]. S. Popescu, C. Ungureanu, A.M. Albu, C. Pirvu. Poly(dopamine) assisted deposition of adherent PPy film on Ti substrate. *Prog Org Coat.* 2014;77(11):1890-900.
- [30]. Q.Q. Lei, Y.W. Zhang, W.N. Zhang, R.W. Li, N.J. Ao, H. Zhang. A synergy between dopamine and electrostatically bound bactericide in a poly (vinyl alcohol) hybrid hydrogel for treating infected wounds. *Carbohydr Polym.* 2021;272.
- [31]. S. Ghalei, H. Handa. A review on antibacterial silk fibroin-based biomaterials: current state and prospects. *Mater Today Chem.* 2022;23.
- [32]. S. Saha, K. Pramanik, A. Biswas. Silk fibroin coated TiO₂ nanotubes for improved osteogenic property of Ti6Al4V bone implants. *Materials Science and Engineering: C.* 2019;105:109982.
- [33]. H. Mezzourh, S. Ben Moumen, M. Amjoud, D. Mezzane, Y. El Amraoui, B. Marbati, A. Lahmar, M. Jouiad, M. El Marssi. Effect of growth time on structural and surface properties of TiO₂ nanostructures deposited by single-step hydrothermal method. *Materials Today: Proceedings.* 2021.
- [34]. T. Tan, Q. Zhao, H. Kuwae, T. Ueno, P. Chen, Y. Tsutsumi, J. Mizuno, T. Hanawa, N. Wakabayashi. Surface properties and biocompatibility of sandblasted and acid-etched titanium–zirconium binary alloys with various compositions. *Dental Materials Journal.* 2022;advpub.
- [35]. V. Anitha, J.-H. Lee, J. Lee, A.N. Banerjee, S.W. Joo, B.K. Min. Biofilm formation on a TiO₂ nanotube with controlled pore diameter and surface wettability. *Nanotechnology.* 2015;26(6):065102.
- [36]. S. Genna, O. Giannini, S. Guarino, G.S. Ponticelli, F. Tagliaferri. Laser texturing of AISI 304 stainless steel: Experimental analysis and genetic algorithm optimisation to control the surface wettability. *The International Journal of Advanced Manufacturing Technology.* 2020;110:3005-22.
- [37]. D. Sun, K.F. Böhringer. Self-Cleaning: From Bio-Inspired Surface Modification to MEMS/Microfluidics System Integration. *Micromachines.* 2019;10(2):101.
- [38]. H. Kim, S.G. Kumbar, S.P. Nukavarapu. Biomaterial-directed cell behavior for tissue engineering. *Current opinion in biomedical engineering.* 2021;17.
- [39]. S.-H. Chiou, H.-C. Ho, H.-T. Liao, F.-Y. Tsai, C.-W. Tsao, Y.-J. Hsu, C.-H. Hsueh. Plasmonic gold nanoplates-decorated ZnO branched nanorods@TiO₂ nanorods heterostructure photoanode for efficient photoelectrochemical water splitting. *Journal of Photochemistry and Photobiology A: Chemistry.* 2023;443:114816.
- [40]. Q. Wang, J. Cai, G.V. Biesold-McGee, J. Huang, Y.H. Ng, H. Sun, J. Wang, Y. Lai, Z. Lin. Silk fibroin-derived nitrogen-doped carbon quantum dots anchored on TiO₂ nanotube arrays for heterogeneous photocatalytic degradation and water splitting. *Nano Energy.* 2020;78:105313.
- [41]. D. Yu, J. Wang, J. Tian, X. Xu, J. Dai, X. Wang. Preparation and characterization of TiO₂/ZnO composite coating on carbon steel surface and its anticorrosive behavior in seawater. *Composites Part B: Engineering.* 2013;46:135-44.
- [42]. C. Zhang, J. Huffer, M. Sprik. Coupling of Surface Chemistry and Electric Double Layer at TiO₂ Electrochemical Interfaces. *J Phys Chem Lett.* 2019;10(14):3871-6.
- [43]. K.M. Thulasi, S.T. Manikkoth, A. Paravannoor, S. Palantavida, B.K. Vijayan. Supercapacitor electrodes based on modified titania nanotube arrays on flexible substrates. 2021;112(12):937-44.
- [44]. W. Bao, Y. Wu, Y. Xie, C. Yao. Fabrication and electrochemical performance of nickel oxide nanoparticles anchored titanium dioxide nanotube array hybrid electrode. *Functional Materials Letters.* 2020;13(04):2051017.
- [45]. R. Bogdanowicz, A. Dettlaff, F. Skiba, K. Trzcinski, M. Szkoda, M. Sobaszek, M. Ficek, B. Dec, L. Macewicz, K. Wyrębski, G. Pasciak, D. Geng, A. Ignaczak, J. Ryl. Enhanced Charge Storage Mechanism and Long-Term Cycling Stability in Diamondized Titania Nanocomposite Supercapacitors Operating in Aqueous Electrolytes. *The Journal of Physical Chemistry C.* 2020;124(29):15698-712.
- [46]. Y. Lin, L. Zhang, Y. Yang, M. Yang, Q. Hong, K. Chang, J. Dai, L. Chen, C. Pan, Y. Hu, L. Quan, Y. Wei, S. Liu, Z. Yang. Loading Gentamicin and Zn²⁺ on TiO₂ Nanotubes to Improve Anticoagulation, Endothelial Cell Growth, and Antibacterial Activities. *Stem Cells International.* 2021;2021:9993247.
- [47]. S. Hussain, M. Khan, T.M.M. Sheikh, M.Z. Mumtaz, T.A. Chohan, S. Shamim, Y. Liu. Zinc Essentiality, Toxicity, and Its Bacterial Bioremediation: A Comprehensive Insight. *Front Microbiol.* 2022;13:900740.

- [48]. *H. Hong, O.J. Lee, Y.J. Lee, J. Lee, O. Ajiteru, H. Lee, Y. Suh, M. Sultan, S. Kim, C. Park.* Cytocompatibility of Modified Silk Fibroin with Glycidyl Methacrylate for Tissue Engineering and Biomedical Applications. *Biomolecules.* 2020;11:35.
- [49]. *M. Cestari, B.S. Caldas, D.P. Fonseca, R.B. Balbinot, D. Lazzarin-Bidóia, I. Otsuka, C.V. Nakamura, R. Borsali, E.C. Muniz.* Silk fibroin nanofibers containing chondroitin sulfate and silver sulfadiazine for wound healing treatment. *Journal of Drug Delivery Science and Technology.* 2022;70:103221.
- [50]. *A.-M. Negrescu, V. Mitran, W. Draghicescu, S. Popescu, C. Pirvu, I. Ionascu, T. Soare, S. Uzun, S.M. Croitoru, A. Cimpean.* TiO₂ Nanotubes Functionalized with Icarin for an Attenuated In Vitro Immune Response and Improved In Vivo Osseointegration. *Journal of Functional Biomaterials.* 2022;13(2):43.